Fall 2021

SEDIMENT TRANSPORT AND THE TEMPORAL STABILITY OF THE SEAFLOOR IN THE HAMPTON-SEABROOK ESTUARY, NH: A NUMERICAL MODEL STUDY

Katherine Vera von Krusenstiern
University of New Hampshire, Durham

SEDIMENT TRANSPORT AND THE TEMPORAL STABILITY OF THE SEAFLOOR IN THE HAMPTON-SEABROOK ESTUARY, NH: A NUMERICAL MODEL STUDY

BY

KATE V. VON KRUSENSTIERN

B.A., Physical Geography, Western Washington University, 2012

THESIS

Submitted to the University of New Hampshire

In Partial Fulfillment of

The Requirements for the Degree of

Master of Science

In

Oceanography

September 2021

This thesis has been examined and approved in partial fulfillment of the requirements for the degree of Master of Science in Oceanography by:

Thesis director, Tom Lippmann

Associate Professor of Earth Sciences and Ocean Engineering

Diane Foster

Director of School of Marine Science and Ocean Engineering

Professor of Ocean Engineering and Mechanical Engineering

John G.W. Kelley,

NOAA Meteorologist and Coastal Modeler

Affiliate Assistant Professor of Ocean Engineering

Larry Ward

Associate Research Professor of Earth Sciences

On May 7th, 2019

Approval signatures are on file with the University of New Hampshire Graduate School

TABLE OF CONTENTS

ACKNOWLEDGEMENTS

This work would not have been possible without the endless support and encouragement from numerous individuals. Thank you to my adviser, Tom Lippmann for the never wavering mentoring and support throughout my project, and to my committee members John Kelly for expertise in numerical modeling, Larry Ward for sediment data and in-depth knowledge of the Hampton-Seabrook study area, and Diane Foster for imparting the knowledge of sediment transport theory. Additionally, thanks to Salme Cook for her tremendous assistance in building a COAWST model framework, grid development, and friendship.

I'd like to acknowledge the various resources made available throughout my degree. The Center of Coastal and Ocean Mapping and the Earth Sciences and Ocean Engineering departments for their support. Jim Irish for assistance with field work and analysis of the observations, John Hunt for field assistance. The expertise from John Warner, Chris Sherwood, and Hernan Arango in developing the COAWST model simulations and implementing the development of hardened structures.

This work was funded by NOAA grant NA15NOS4000200. Model simulations are performed on supercomputer supported by the NSD MRI Program under grant PHY-1229408.

LIST OF TABLES

Table **Page**

LIST OF FIGURES

ABSTRACT

Observations of sediment transport pathways and bathymetric change are often difficult to obtain over spatial and temporal scales needed to maintain economic and ecological viability in dynamic coastal and estuarine environments. As a consequence, numerical models have become a useful tool to examine the sediment transport and evolution of inlets, estuaries, and harbors. In this work, sediment transport at the Hampton-Seabrook Estuary (HSE) in southern New Hampshire is simulated using the Coupled Ocean Atmospheric Waves and Sediment Transport (COAWST) modeling framework to assess bathymetric change over a 5-year period from September 2011 to November 2016. Initial bathymetry and sediment grain size distribution are established from observations and smoothed onto a 30 *m* rectilinear grid that encompasses the entirety of the HSE system and extends two *km* offshore into the Gulf of Maine. Careful consideration is made to include hardened structures, such as jetties and sub-surface bulkheads, into the model framework. The model is forced with observations of water levels (including subtidal and tidal motions) from a local tide gauge. Field observations of sea surface height and currents are used to validate model hydrodynamics and establish bottom boundary conditions. The verified model predicts bathymetric change in the harbor consistent with observed changes obtained from bathymetric surveys conducted at the beginning and end of the five-year study. Of particular interest is a cut through the middle ground of the flood tidal delta and the filling in of the navigational channel leading to the Seabrook side of the Harbor that is qualitatively well reproduced by the model. In general, the model qualitatively well-predicts the gross 5-year evolution of the flood tidal delta and the channels leading to the upstream rivers suggesting that hydrodynamically-verified numerical models can be used to qualitatively predict depositional and erosional regions over inter-annual time scales at Hampton Harbor.

CHAPTER 1

INTRODUCTION

In dynamic, shallow-water coastal areas, wave and current induced sediment transport and subsequent morphologic change to the seafloor are difficult to observe *in situ* on spatial and temporal scales that quantify changes to shallow bathymetry. Man-made structures (*e.g.*, jetties) constructed to control coastal dynamics and additional climate change-induced consequences (*e.g.,* sea-level rise) add complexity to the problem and limit our ability to understand feedback between human activities and the physical system. However, changes in bathymetry caused by seabed erosion or infilling (deposition) of navigable areas can often disrupt the economic and natural function of coastal areas. The coastal zone supports vital navigational routes, coastal infrastructure, and natural resources, all dependent on changes to sub-tidal topography; thus, it is necessary to identify controls and magnitudes of sediment transport to understand morphologic evolution and predict bathymetric change to support resilient coastal communities.

Evaluating geomorphic evolution of the seafloor in shallow water areas is commonly achieved by directly differencing two successive surveys completed at distinct times t_1, and t_2,

$$\Delta Z = Z(x, y, t_1) - Z(x, y, t_2) \quad (1)$$

where Z is bathymetric depth, and x and y are the horizontal Cartesian coordinate. Spatial maps of the bathymetric difference, ΔZ, depict areas of erosion (net loss of sediments) and deposition (net gains in sediments), changes to the coastline, or changes to tidal channels and inlets. Repeated surveys inform longer-term trends about the sediment dynamics of a study area. Such empirical studies may be used, for example, to guide dredging decisions ensuring safety to mariners in

navigable channels, or to allow coastal managers to better manage the economical and natural resources of the area. However, in practice, economic and logistical constraints can limit the feasibility of conducting time consuming and expensive regular bathymetric surveys.

Currently, high-resolution bathymetric surveys in shallow, coastal areas are usually conducted using ship-mounted acoustic multi-beam and single beam sonar systems or with airborne optical Light Imaging Detection and Ranging (LIDaR) systems. Both technologies come with setbacks. For example, ship-based acoustic bathymetry systems often are unable to directly survey in shallower depths typical of estuarine environments (< 1-10 m) due to the draft of the vessel and can be limited by surface wave and current conditions. Optical LIDaR technologies become less accurate in deeper water depths or under turbid, sediment-laden conditions where laser pulses are attenuated and reflections from the seabed are not resolved in the back-scattered waveform. Moreover, both methods can be cost-prohibitive thus reducing how often repeat surveys can be conducted, limiting robust time-sensitive detection in highly dynamic coastal areas such as beaches, inlets, and harbors.

In the absence of repeated and timely high-resolution seabed surveys, coastal scientists and engineers have turned to numerical shallow water hydrodynamic models (that simulate waves and currents) coupled with sediment transport models to simulate morphodynamic evolution over varying temporal and spatial scales. On weekly and monthly time-scales, realistic numerical model simulations have compared well to observations of storm-induced sediment transport in nearshore environments in both three dimensions (*e.g.*, Warner, *et al*., 2010; Ganju, *et al*., 2016) and two-dimensions (*e.g.*, Hopkins, *et al*., 2018). On longer time scales over a seven-month period, Moriarty, *et al.* (2014) demonstrated high skill using a three-dimensional hydrodynamic–sediment transport numerical model to track sediment dispersal from river output along the continental shelf.

Many coastal sediment and transport models link finer scale sediment transport processes to larger scale geomorphic evolution using a heuristic morphological acceleration model factor (MF) to accelerate bed-level updating and to reduce the computational cost of simulations over long periods of time (Lesser, *et al.*, 2004; Luijendijk, *et al.*, 2019). For example, Luan, *et al*. (2017) applied an MF in Delft3D to hindcast and forecast erosion and deposition patterns over decadal time-scales of the Yangtze Estuary using multiple sediment size fractions and with variations in river flow and sediment discharge. Results indicated that modeled patterns of morphological change qualitatively agreed with observations and the study successfully applied the validated model to forecast future sediment transport trends of the estuary. Likewise, Ganju and Schoellhamer (2010) forecasted decadal geomorphic change in Suisun Bay, California under different climate scenarios using ROMS, a coupled hydrodynamic-sediment transport model. Such studies elucidate dominate processes of morphologic forcing and allow for forecasting future evolution patterns.

The advent of increased computational resources and publically available models has given rise to application of high-resolution numerical modeling studies to a variety of coastal areas without MF acceleration factors (*e.g*., Roelvink and Reniers, 2012, and references therein). These seafloor change detection studies have been shown to have some skill in simulating morphodynamic change over short (< 1 *yr*) and long (> 1 *yr*) time scales, and are now significant tools in elucidating sediment transport processes in dynamic, coastal waters, particularly at higher temporal resolution than can be tested with repeat bathymetric surveys.

In this work, we apply a coupled hydrodynamic and sediment transport model to the Hampton-Seabrook Estuary (HSE) over a five-year period to test the model's ability to reproduce observed temporal changes to the seafloor. HSE is a tidally-dominated, back-barrier estuary in the

southern Gulf of Maine with a dynamic sediment transport regime (Randall, 1989; Kedzierski, 1993; Ward, *et al.*, 2013; Ward and Irish, 2014; Figure 1.1). Of particular interest to HSE is the significant shoaling and sediment redistribution within the back bay and inlet that requires regular dredging of navigational waterways and anchorages to maintain safe passageways (Kedzierski, 1993; PDA, 2012). As the local center for New Hampshire commercial and recreational fishing, forecasting sediment transport patterns and morphologic evolution of the seafloor over inter-annual time-scales is important to the livelihood and economic viability of the region (*e.g.*, Eberhardt and Burdick, 2008).

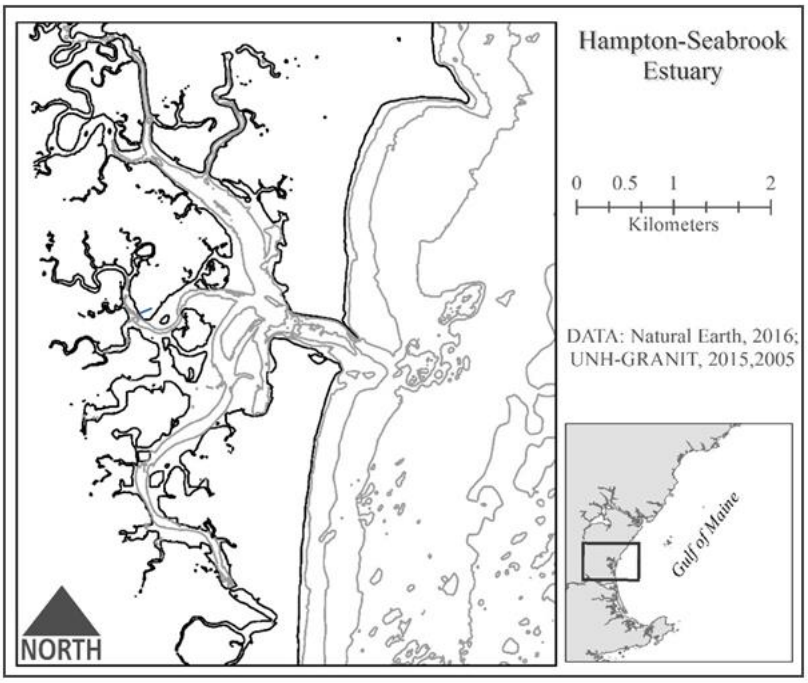

Figure 1.1*:* Hampton-Seabrook Estuary, New Hampshire, U.S. Light contours show the 2, 5, 10, and 20 *m* bathymetry intervals. Insert map shows the study location within the southern Gulf of Maine. Data from Natural Earth, 2016, and UNH-GRANIT 2005 and 2015.

Observations of HSE bathymetry over a five-year interval from 2011-2016 (discussed herein) reveal large changes to the flood tidal delta and various channels leading into the extensive back bay salt marshes. Of particular importance is a newly cut channel through the flood tidal

delta and the infilling of the navigation channel leading to the principal moorage for the fishing fleet and commercial tourism vessels. Figure 1.2 shows a Google Earth satellite image from 2005 after the construction of sub-tidal bulkheads (described later in more detail) compared with a recent aerial photograph of the same area in 2017. Although the bulkheads alleviated the chronic erosion problem along the southern shore of the harbor (Figure 1.2a), a new cut across the flood tidal delta resulted in sediment infilling of the navigational channel to the harbor (Figure 1.2b), and necessitating emergency dredging operations. In this work, a coupled hydrodynamic and sediment transport numerical model is used to simulate the 5-year bathymetric change observed qualitatively in Figure 1.2. Model simulations are compared with the observed bathymetric changes from the bathymetric surveys. Sensitivity to critical bed shear stress and erodibility model parameters are examined with repeated simulations.

Figure 1.2: (A) 2005 satellite imagery post construction of sub-tidal bulkheads along the southern shore of the harbor. (B) 2017 oblique airborne imagery showing rearrangement of the flood tidal delta, cut across the Middle Ground, and active sedimentation of navigational channel leading into the Seabrook Harbor mooring area. Satellite imagery from Google Earth. Airborne image from the USACE.

Section 2 describes the geographical setting and previous research of the HSE study area. Section 3 describes the modeling system and the numerical methodologies. Section 4 examines how the model results compare to the observations. Section 5 discusses the results in terms of sediment transport patterns and morphologic change, as well as applicability of numerical modeling techniques to observing seafloor evolution and modeling limitations. Section 6 summarizes the conclusions.

CHAPTER 2

STUDY SITE

2.1 Physical Setting

The Hampton-Seabrook Estuary is a tidally-dominated, back-barrier estuary located in southern New Hampshire, USA, and is connected to the Gulf of Maine by the Hampton Inlet (Figure 1.1*).* Two sandy barrier beaches to the north and south separate the back-barrier from the Atlantic Ocean, with the only ocean water exchange occurring through Hampton Inlet. The estuary is typical of many systems along the western Gulf of Maine, similarly characterized by tidal mudflats and expansive salt marshes.

HSE is a mesotidal system with a semi-diurnal tide ranging 2-4 *m* during neap and spring periods (*e.g.,* McKenna, 2012). The swiftest currents occur within the inlet, reaching 1.5-2 *m*/*s* during peak flows with typical back bay currents in tidal channels ranging 0.5-1.0 *m*/*s* (Lippmann, *et al*., 2020). Although the back-bay is fed by five tidal rivers, the Hampton River and Taylor River to the north, Mill Creek and Browns River to the west, the Black Water River to the south, and numerous tidal creeks, the total mean freshwater discharge is estimated to be 0.12 $m^3\ s^{-1}$ (NHDES, 1994), and is considered to have negligible impact on estuarine dynamics (Letter, *et al*., 2005).

Locally, HSE is an important economic and ecological center. The tidal wetlands support a diverse habitat, including the largest clam industry in the state (NHDES, 1994). Two harbors located within the estuary, Hampton Harbor to the north and Seabrook Harbor to the south, house

the largest commercial fishing fleet in the state, and is heavily used by recreational boaters, charter fishing, and whale-watching outfits (Hall-Arber, *et al.*, 2001). Vessel traffic is high, particularly in the summer months, with ample dedicated moorings and marine services. State and local authorities prioritize the health and function of the estuary to support the coastal NH economy (PREP, 2019).

The estuary has a dynamic sediment transport regime dominated by tidally-driven currents, with frequent shoal reconfiguration and sediment infill of waterways and harbors (Kedzierski, 1993). The southern domain of the estuary is less stable than the northern, with frequent migration of tidal channels through the primary flood shoal – locally known as the Middle Ground – where the Black Water River meets the back-bay (Letter, *et al*., 2005). Dense vegetation of the salt marsh reduces the momentum of the water, resulting in enhanced sedimentation of fine sands and mud during flood tides (Letter, *et al*., 2005). Migration of tidal channels is generally slow but can contribute sediment to the continuously changing seabed in the back-bay. Numerous field studies on sediment grain size distribution indicate the estuary is largely sand dominated (0 φ to -1 φ, 2 *mm* to 4 *mm*), particularly on the beaches, inlet and back barrier shoals (Letter, *et al*., 2005; Ward, 2007; Ward, *et al*., 2015). The proportion of mud (8 φ to 4 φ) increases upstream as distance from the inlet increases.

Due to the mobile nature of the sediment, the USACE actively work to reduce the impact of sedimentation on the economic function of the estuary. Human intervention on the natural system began in the 1930s with construction of the north and south jetties on either side of the inlet, built originally to reduce sedimentation within the inlet (discussed in Mahmutoglu, 2001). In the 1940s, dredging of the anchorage areas and navigational waterways began, a process that regularly continues today to maintain navigational safety. In the 1990s a significant alteration to the estuary

was established to alleviate severe erosion of the shoreline along the southern end of the back-bay and infilling of the Seabrook Harbor mooring channel.

Following hydrodynamic studies (Mahmutaglu, 2001; and discussed in Letter, *et al.*, 2005, and Leung, 2007), in 2004 a coastline protection system (known as Section 227) was built by the USACE National Shoreline Derision Control Development and Demonstration Program in efforts to mitigate what is known as the River Street Cut, a reconfiguration of the tidal channel through Middle Ground (Figure 2.1. This breach created a new channel for the outflow of the Black Water River adjacent to waterfront homes along River Street. Increased velocities associated with this nascent channel increased erosion, threatening the stability of the private homes. Furthermore, velocity differences between the channel and Seabrook Harbor promoted sediment deposition in Seabrook Harbor, reducing anchorage possibilities for recreational and fishing vessels. Under Section 227, Seabrook Harbor was dredged and the resulting sediment was used to fill in the River Street Cut. Subsurface bulkheads constructed of dual vinyl sheet piles were built on either side of the cut to retain the fill and reduce future erosion (Letter, *et al*., 2005). This system was successful for many years and has alleviated the erosion problems along River Street; however, recently a new cut across the Middle Ground beginning at the end of the bulkheads resulted in significant infilling once again of the navigational channel that provides access to the anchorage (Figure 2.1).

2.2 Previous Modeling Efforts

As part of the Section 227 plan, the University of New Hampshire was commissioned to develop a hydrodynamic numerical model of the system that included a field study to calibrate and validate model results. This 2005 study (Letter, *et al*., 2005) utilized a two-dimensional, depth-averaged, finite element hydrodynamic model, RMA-2, to evaluate changes in sea-surface heights

and tidal currents where the Black Water River flowed into Seabrook Harbor under different dredging scenarios (Mahmutoglu, 2001; Leung, 2007). Model-predicted depth-averaged currents and sea surface elevation due to tidal forcing during the spring tides were validated against the field observations. Sensitivity analysis included tuning of bottom friction and turbulence mixing parameters.

The resulting model was updated by the USACE to include a two-dimensional sediment transport model, SED-2D, to predict longer term shoaling in the estuary (Letter, *et al*., 2005). The SED-2D model calculates both bedload and suspended sediment transport using the Acker-White total load equations for a single representative sediment grain size. Results indicated sediment deposition in the ebb lee of the piers and an increase in sedimentation at the entrance of the harbor (Letter, *et al*., 2005). While no further numerical studies followed these initial results, the HSE system has been continuously monitored and dredged when needed.

Since the advent of the modeling studies conducted in the 1990s, significant advancements have been made to numerical modeling systems and computing resources. Today there are many publically available numerical models that couple three-dimensional hydrodynamics with state-of-the-art sediment transport formulations (ADCIRC: Luettich, *et al.*, 1992; FVCOM: Chen, *et al.*, 2003; Delft3D: Lesser, *et al.*, 2004; COAWST: Warner, *et al.*, 2010). These advancements allow more detailed evaluation of the hydrodynamics resolving vertically varying flow fields, implementation of improved understanding of sediment transport under a range of sediment size classes, and incorporation of man-made physical structures within the numerical grid. Access to supercomputing resources allow significant extension of model simulations to much longer monthly to inter-annual time periods with small, O(1 *s*), time steps without the need for morphological acceleration parameters.

CHAPTER 3

METHODS

In this work, the Coupled-Ocean-Atmospheric-Wave-Sediment Transport (COAWST) modeling system is used to simulate the hydrodynamics and sediment transport (discussed later). Five-year hindcast simulations include non-cohesive transport formulations to investigate erosional and depositional patterns at HSE. The model is calibrated with observations of vertically varying horizontal currents and sea surface elevation obtained over a 40-day spring-neap tidal cycle. Bathymetric change simulated by the model is compared with the observed change obtained from two surveys separated by a five-year period (2011-2016).

Field observations (described in section 3.1) include a 2016 single-beam bathymetric survey of the back-bay and inlet, and a 40-day field experiment conducted in 2017 with current profilers and pressure sensors deployed at 9 different locations within the estuary. The COAWST modeling framework is described in section 3.2. The numerical grid and model set-up is defined in section 3.3, and the suite of simulations described in section 3.4.

3.1 Field Observations

In October-November 2016, the bathymetry of the back bay and inlet was measured with the Coastal Bathymetry Survey System (CBASS; Lippmann and Smith, 2009). The CBASS is a 1998 Yamaha Waverunner personal watercraft equipped with a 192 *kHz* single-beam acoustic echo-sounder, differential GPS, and custom navigation system. The CBASS can survey in water depths less than 1 *m* with seabed elevation accuracy of 0.07 to 0.10 *m*. The high maneuverability and

shallow draft allowed for accurate mapping of the shallow, upstream areas, along pre-defined transect lines separated by 20 *m* (Figure 3.1). Raw data were filtered to remove spurious soundings gridded to 10-30 *m* horizontal resolution with a Delauny triangulation and linear interpolation for model grid development.

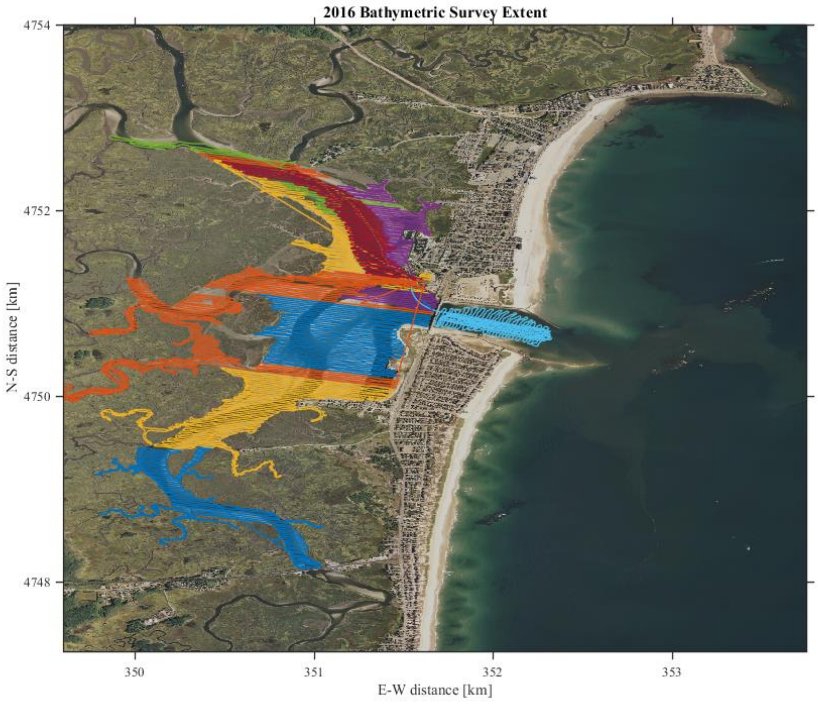

Figure 3.1: Survey transect lines with approximately 20 m spacing spanning the study area used for the 2016 shallow water mapping with the CBASS. Colors indicate the different lines covered on any given day.

A hydrodynamic field study was conducted from 3 November 2017 to 8 December 2017 to obtain currents and water levels to validate the numerical model. Nine locations within the inlet were instrumented with bottom tripods and various frames (Figure 3.2). Instrumentation deployed includes five acoustic Doppler current meters with pressure sensors and four other bottom mounted pressure sensors. All data were averaged over the same 30 minute intervals for the duration of the experiment.

Currents and pressure were measured with two Teledyne RD Instruments 1200 *kHz* Workhorse acoustic Doppler current profilers (ADCP) with pressure sensors, the first placed just seaward of the inlet in 6.4 *m* water and the second inside the inlet in 3.5 *m* water depth, close to the flood delta tidal shoal. Currents and pressures were sampled at 1 *Hz* in 0.5 *m* depth bins spanning the water column. A Sontek Argonaut ADCP was deployed in the upper reaches of Mills Creek in 3.7 *m* water depth, and also sampled currents at 1 *Hz* in 1 *m* depth bins. A Nortek single-point Aquadopp acoustic Doppler velocimeter (ADV) was deployed in about 3.8 *m* water depth upstream in Taylor River and measured velocities and pressures about 70 *cm* above the bed. A Nortek AquaPro ADCP was placed near the Rt. 286 Bridge in the Black Water River and recorded velocities at 1 *Hz* in 25 *cm* vertical bins (no pressure sensor record was recovered from the instrument).

In addition to the pressure records obtained from the ADCPs and ADV, four Sea-Bird Electronic instruments (3 SBE-39 and 1 SeaCat16+) were placed in the Taylor River, Mills Creek, Black Water Rivers, and near Chouinards Pier in the back-bay in water depths of 3.6 *m*, 2.8 *m*, 1.7 *m*, and 2.5 *m*, respectively. All pressure records were used to estimate the tidal amplitudes and were not used for absolute mean sea surface elevations (*i.e.*, no set-up of the water levels was considered).

Sediment grain size was determined from 112 surface grab samples collected from 2005 to 2016 as part of ongoing studies of sediment composition in the HSE, including Hampton and Seabrook Beach (Ward, *et al.*, 2015; Figure 3.3). These data are used to establish the heterogeneity of sediment within the study area by defining the spatially variable initial grain size characteristics used in sediment transport formulations.

Figure 3.2: Instrument locations within study area. A – 1200 kHz RDI ADCP; B – 1200 kHz RDI ADCP; D – SBE39 pressure sensor; E – 3000 kHz Sontek Argonaut ADCP; F – SBE30 pressure sensor; G – Nortek Aquapro ADV; H – SBE39 pressure sensor; I – 1000 kHz Nortek Aquapro ADP; J – SBE19 and Nortek Vector ADV.

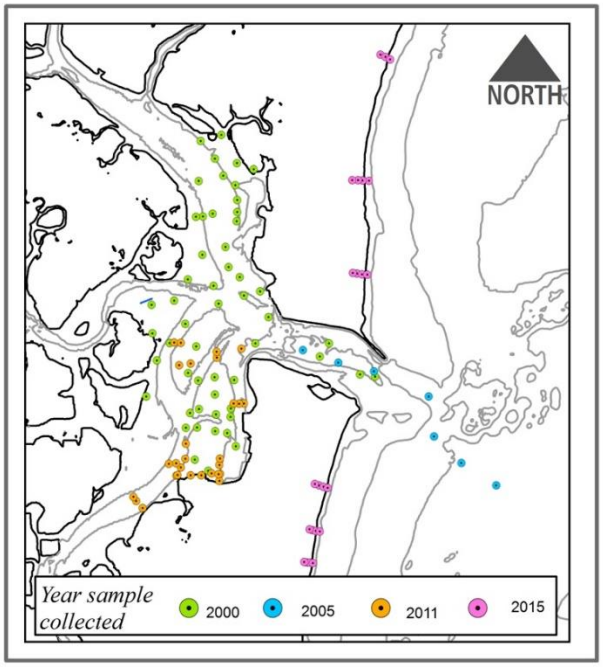

Figure 3.3: Locations of sediment grab samples within study area. Corresponding collection dates listed in the legend.

3.2 Numerical Model

The COAWST numerical modeling system (Warner, *et al.*, 2010) couples four open-sourced models – the hydrodynamic Regional Ocean Model System (ROMS; Haidvogel *et al.,* 2008; Shechepetkin and McWilliams, 2005), the atmospheric Weather Research Forecasting model (WRF; Skamarock, *et al.*, 2005), the wave model Simulating WAves Nearshore (SWAN; Booij, *et al.*, 1999), and the Coastal Sediment Transport Model (CSTM; Warner, *et al.*, 2008a) through the Modeling Coupling Toolkit (MCT; Warner, *et al.*, 2008b). Wetting and drying algorithms allow for the inundation and dewatering of model cells (Warner, *et al.*, 2013). In this work only ROMS and CSTM were utilized as ocean waves and winds were not considered in the model. Surface gravity waves emanating from offshore are refracted laterally over the ebb shoals along the southern end of the inlet and strongly attenuated through the inlet mouth, and were assumed to

have relatively little influence on the back-bay sediment transport (the focus of this study). Sediment transport along the adjacent beaches is dominated by waves and wave-driven currents, but was not included in the present model. In essence, the sediment transport along the beach was assumed to have no influence on the sedimentation of the harbor over the 5-year study. Winds over the back-bay area can generate waves but these tend to by small and were also assumed to produce negligible seabed orbital velocities compared to the strong tidal currents that dominate the hydrodynamic flows.

ROMS models have been widely used in coastal applications including a number of estuaries similar to HSE and shown to well-predict the tidal hydrodynamics (Warner *et al.,* 2005; Ganju, *et al.,* 2017, Cook, *et al*., 2019). In this study, the coupled hydrodynamics (ROMS) and sediment transport (CSTM) models in COAWST are used to hindcast the effect of tidal forcing on erosion and deposition in HSE over the five-year study period. Formulation of the governing equations for the ROMS and CSTM model are summarized below (details can be found in Warner, *et al.*, 2008a, 2010).

Regional Ocean Modeling System

ROMS is a three-dimensional, free surface, terrain following, finite difference, ocean circulation numerical model that solves the Reynolds-averaged Navier-Stokes (RANS) equations using the hydrostatic and Boussinesq assumptions (Haidvogel, *et al*., 2008). The equations are discretized into an orthogonal Arakawa C grid in the horizontal direction and on sigma (terrain-following) coordinates in the vertical. The barotropic and baroclinic hydrodynamic components are propagated forward in time using a split-explicit time-stepping algorithm (Shchepetkin and McWilliams, 2005). Within each baroclinic time-stepping interval there are a finite number of barotropic time steps that each solve the depth-integrated equations of motions.

The ROMS modelling framework is rooted in adaptability to fit the physical problem described, thus the structure allows multiple choices to solve many model components. There are several options for advection schemes and boundary conditions (Warner, *et al*., 2010). Furthermore, treatment of physical processes that vary over temporal and spatial scales not resolved by the model domain – Reynolds stresses, turbulence processes, and bottom boundary layer dynamics – are parameterized through selection of eddy viscosity, K_M, and horizontal and vertical diffusivity, K_H and K_V, model coefficients.

Momentum, scalar advection, and diffusive processes are solved using transport equations, and the density field is determined using an equation-of-state that accounts for temperature, salinity, and suspended sediment concentrations. The governing momentum equations, continuity equation, and scalar transport equation in Cartesian horizontal and sigma vertical coordinates are well known and described in detail in Warner, *et al*. (2010). Turbulence closure schemes utilized include the Mellor-Yamada 2.5 and generic length scale (GLS) methods (Warner, *et al*., 2005; Shchepetkin and McWilliams, 2005).

The shear stress at the seafloor has a first order effect on the hydrodynamic and sediment transport behavior. The bottom stress in the horizontal directions defines the bottom boundary conditions in the RANS momentum equations. The effective bottom stress influences both the rate of sediment resuspension into the water column, and the bedload transport rate (Haidvogel, *et al.*, 2008; Warner, *et al*., 2008a). How the sub-grid scale processes are parameterized in the bottom boundary layer (BBL) has important consequences to the overall solution of the numerical model. Within ROMS, description of the BBL processes is differentiated by analytical drag-coefficient expressions, or formulations representing wave-current interactions over dynamic seabed roughness elements.

Bottom stress, τ_b, is parameterized in the bottom grid cell by a quadratic drag coefficient, C_D, such that

$$\tau_b = C_D U|U| \tag{2}$$

where $|U| = \sqrt{u^2 + v^2}$ is the total flow velocity with *u* and *v* the orthogonal velocity components in the *x* and *y* directions, respectively. The vertical variation in flow velocity is assumed to follow a classic logarithmic profile,

$$|U| = \frac{u_*}{\kappa} \ln(\frac{z}{z_0}) \tag{3}$$

where the friction velocity $u_* = \sqrt{|\tau_{bx}| + |\tau_{by}|}$, z is the elevation above the seafloor (in this case the mid-elevation point of the bottom grid cell), $\kappa = 0.41$ is von Karman's constant, and z_0 is the bottom roughness length (in *m*). The kinematic bottom stresses in the *x* and *y* directions, τ_{bx} and τ_{by} are given by

$$|\tau_{bx}| = \frac{\kappa^2 u\sqrt{u^2+v^2}}{ln^2(\frac{z}{z_0})} \tag{4}$$

$$|\tau_{by}| = \frac{\kappa^2 b\sqrt{u^2+v^2}}{ln^2(\frac{z}{z_0})} \tag{5}$$

In the above formulation, roughness length z_0 is an explicitly defined bottom roughness length scale that parameterizes the drag on the flow associated with grain roughness, saltating grains, and subgrid scale bottom topography. When representing the BBL in the lowest grid cell with a constant drag-coefficient, z_o also remains constant in time, but can be uniform or spatially distributed within the model domain. More complicated methods (not used herein) include wave and current interactions that determine the BBL and include spatially and temporally updating bottom roughness formulations (Ganju and Sherwood, 2010).

The interior (back-bay) lateral boundary conditions were defined as closed, and the ocean boundary defined by an open boundary condition for sea surface height, velocities, and particles. An implicit Chapman condition (Chapman, 1985) was applied to sea surface height in conjunction with a Flather condition (Flather, 1976) for 2D momentum to account for the wave motions (tides) that exit the domain at the shallow water phase speed. Radiation and gradient boundary conditions eliminate reflections of velocity components that deviate from the gravity wave relationships and allow tracers and momentum to leave the domain (Marchesiello, *et al*., 2001).

Community Sediment Transport System

The CSTS model provides routines for sediment transport, and feeds bottom stress calculations and updated bathymetry back to the hydrodynamic components in ROMS. Formulations account for both suspended sediment and bedload transport of a user-defined discretization of sediment grain size classes, as well as a dynamic sediment bed tracking time-evolving morphology and stratigraphy. While sediment classes are distinguished between cohesive and non-cohesive sediments, each corresponding to individual formulations (Tarpley, *et al.*, 2019), this work only considers non-cohesive sediments.

The sediment module is broken down into three primary components: non-evolving individual grain sizes and their attributes, a two-dimensional array describing the evolving bulk-properties of the sediment bed, and a three-dimensional sediment bed. Both the two-dimensional and three-dimensional arrays are updated each time-step, while individual grain size characteristics remain constant and uniform. Each defined sediment grain size is assigned a diameter, density, fall velocity, critical shear stress for erosion, and erodibility constant. The individual grain attributes determine the two-dimensional bulk properties of the sediment bed, including mean grain diameter, mean density, mean settling velocity, and mean critical shear stress for erosion.

Sub-grid morphology (small-scale bedforms) contribute to the bottom roughness length scale and are parameterized with bulk properties of the seabed.

The sediment bed itself is a three-dimensional array with a user-defined number of layers beneath each horizontal model cell. Each cell of each layer is initialized by the user with a porosity, bed thickness, age, and fraction of defined sediment classes. This information, combined with the mean density of the sediment classes make up the mass of each cell. Bed layers evolve with each time-step via bedload and suspended sediment transport. The amount of sediment available to bedload transport, exchanged horizontally between the top layers of the bed, is limited to the amount of mass in the top layer. Suspended transport of sediment, exchanged between the top bed layer and the water column, is limited to the availability of sediment mass in the active layer thickness, z_a, calculated at each time-step following Harris and Wiberg (1997)

$$z_a = \max\left[0.007\left(\tau_{sf} - \tau_{ce}\right)\rho_0, 0\right] + 6.0D_{50} \qquad (6)$$

where τ_{sf} is the maximum bottom shear stress, τ_{ce} is the averaged critical shear stress for erosion (determined by the grain size; described later), and D_{50} is the median grain diameter of the surface sediment. If the bed layer is thicker than z_a, its size is not altered. However, if the top layer is less than the computed active layer thickness, then sediment mass from deeper layers in entrained into the top layer until the top layer is equal to z_a. Thus, the top layer is always at least equal to z_a. In this way, the stratigraphy of the sediment bed can be tracked. In the numerical simulation, the active-layer thickness z_a is calculated first. Then after erosion and deposition are accounted for in a given sediment bed cell, the two-dimension sediment characteristics are updated.

Suspended sediment is transported by solving the advection-diffusion equation with an additional source/sink term to account for sediments settling out of the water column and the

vertical flux of sediment into the water column, represented by the erosion flux, E_s (Warner, *et al*., 2008a), given by

$$E_s = E_0(1-\varphi)\frac{\tau_{sf}-\tau_{ce}}{\tau_{ce}}, when\ \tau_{sf} > \tau_{ce} \quad (7)$$

Erosion flux represents the mass of sediment resuspended into the water column (in $kg\ m^{-2}\ s^{-1}$), controlled by two explicitly defined coefficients: an empirical bed erodibility constant E_0 and the sediment bed porosity φ.

For advection of sediment and other tracers (*i.e*., temperature), ROMS includes numerous high-order accuracy, non-oscillatory, and mass conserving schemes. Amongst these include two positive definite advection schemes – multidimensional positive definite advection transport algorithm (MP-DATA) and the high-order spatial interpolation at the middle temporal level coupled with a total variation diminishing scheme (HSIMT-TVD), both of which are suited for transport of suspended sediment (Wu and Zhu, 2010). In the vertical, advection is calculated with a piece-wise parabolic method, including a weighted non-oscillatory scheme (Warner, *et al*., 2005).

Within the CTSM, bedload transport is calculated for unidirectional flow following the Meyer-Peter Mueller (1948) formulation, or for the combined effect of waves and currents following the Soulsby and Damgaard (2005) formulation. Both routines are a function of sediment density, grain size, and critical shear stress, where non-dimensional sediment transport rates, Φ, are calculated for each defined grain-size and then represented by a quantitative bed-load transport rate, q_{bl}

$$q_{bl} = \Phi \sqrt{\left(\frac{\rho_s}{\rho} - 1\right) g D_{50}^3 \rho_s} \quad (8)$$

where $\left(\frac{\rho_s}{\rho} - 1\right)$ is the submerged sediment weight with ρ the density of water and ρ_s the density of the grains, and D_{50} is the median grain diameter. Total bedload flux for each sediment class is limited to the available mass in the top bed layer. At each time-step, flux differences account for the change in sediment mass in the bed due to transport. Here, the Meyer-Peter Mueller formulation is considered.

Under the Meyer-Peter Mueller routines, the magnitude of the non-dimensional transport rate, Φ, is calculated for each sediment class at the cell faces as a function the non-dimensional shields parameter, and then interpolated to cell centers following Soulsby and Damgaard (2005) and detailed in Warner, *et al*. (2008a). The transport rate is given by

$$\Phi = \max[8(\theta_{sf} - \theta_c)^{1.5}, 0] \quad (9)$$

where θ_c = 0.047 represents the critical Shields parameter. θ_{sf} is the non-dimensional Shields parameter given by

$$\theta_{sf} = \frac{\tau_{sf}}{\left(\frac{\rho_s}{\rho} - 1\right) g D_{50}} \quad (10)$$

where τ_{sf} is the total magnitude of the skin-friction component of the *x* and *y* components of the bottom stress,

$$\tau_{sf} = \sqrt{\tau_{bx}^2 + \tau_{by}^2} \quad (11)$$

3.3 Model Setup

Within the COAWST framework, ROMS and CSTM routines are used to investigate seafloor morphology change to HSE over a five-year time span. The model solution is forced by observations of sea surface heights on the eastern (open ocean) boundary of the domain in the Gulf of Maine. Creating a numerical model for HSE requires defining the horizontal and vertical

resolution of the domain, establishing an initial bathymetry, applying appropriate forcing, and specifying boundary conditions. Due to the abundance of methods to parameterize physical processes in both ROMS and CSTM routines, there are many explicitly defined coefficients and parameters that can be tuned to represent the physical processes of any specific study area. Consequently, creating a feasible model becomes an iterative process whereby a model simulation is performed many times to examine sensitivities to certain variables by comparing the result with field observations.

Simulations were performed on a rectilinear grid with 30 m horizontal resolution (Figure 3.4), and eight vertical, terrain-following, sigma layers. The domain encompasses the tidally inundated HSE including barrier beaches and inlet, and extends seaward roughly 2 km. Depths offshore extend to 30 m (NAVD88) and range 0-6 m within the back-bay while allowing for inundation of subaerial profiles along the water's edge (accounted for with wetting and drying algorithms). The model domain also includes upland elevations up to 20 m.

Vertical resolution varies in the domain and depends on the water depth (*i.e.*, the depth changes but the number of vertical layers stays the same). In shallow water applications, this transformation function behaves like equally spaced sigma coordinates when $h(x, y, t) < h_c$, absolving unnecessarily high resolution and the associated CFL limitation and reduces pressure gradient errors (Shchepetkin and McWilliams, 2005). The vertical transformation and stretching function for simulations in HSE are configured to enhance bottom boundary resolution, as well as limit violations of the CFL condition or inaccuracies in the pressure gradient. The vertical discretization of the water column is updated each time-step as total depth is changing due to tidal variations in the sea surface elevation and erosional/depositional processes at the seabed.

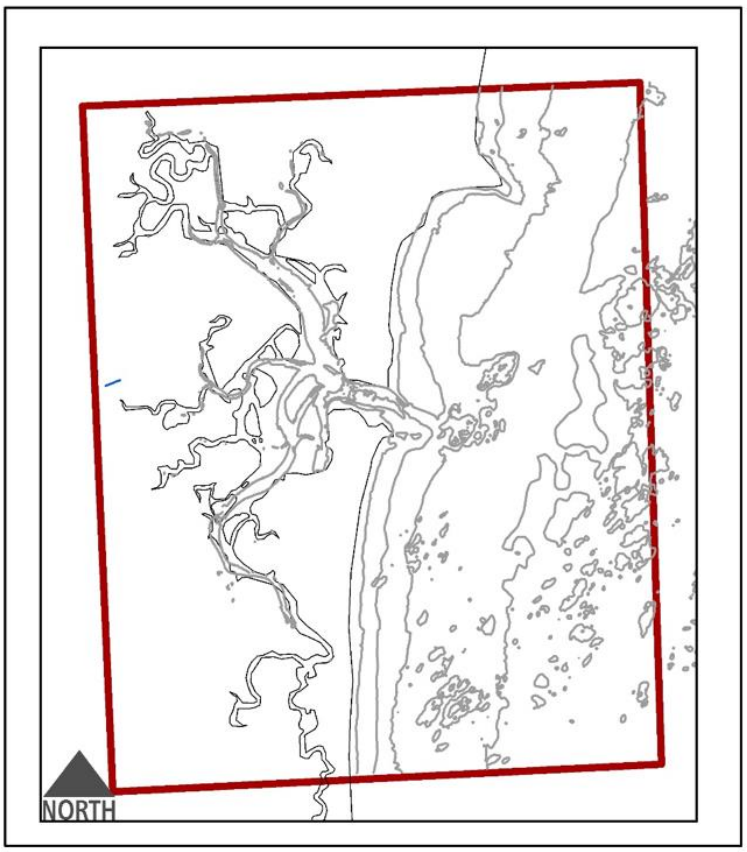

Figure 3.4: Model domain for the simulations (red bounding box). Grid resolution is 30 m, with 8 vertical sigma layers. The model is forced along the right-hand boundary.

Initial Bathymetry and Bed Characteristics

The reliability of a numerical model solution depends on the accuracy of the input bathymetry and forcing data; without good initial bathymetry, simulations will not accurately reproduce the flow. To best represent bathymetry for the HSE study area, seven different surveys were merged together into a single, comprehensive grid (Figure 3.5). Data sources and their respective spatial coverage are described in Appendix A. Herein the 'bathymetry grid' collectively refers to both ocean and land elevations. Location of coastal structures within the study domain, such as jetties, are accounted for in the set-up of the initial grid.

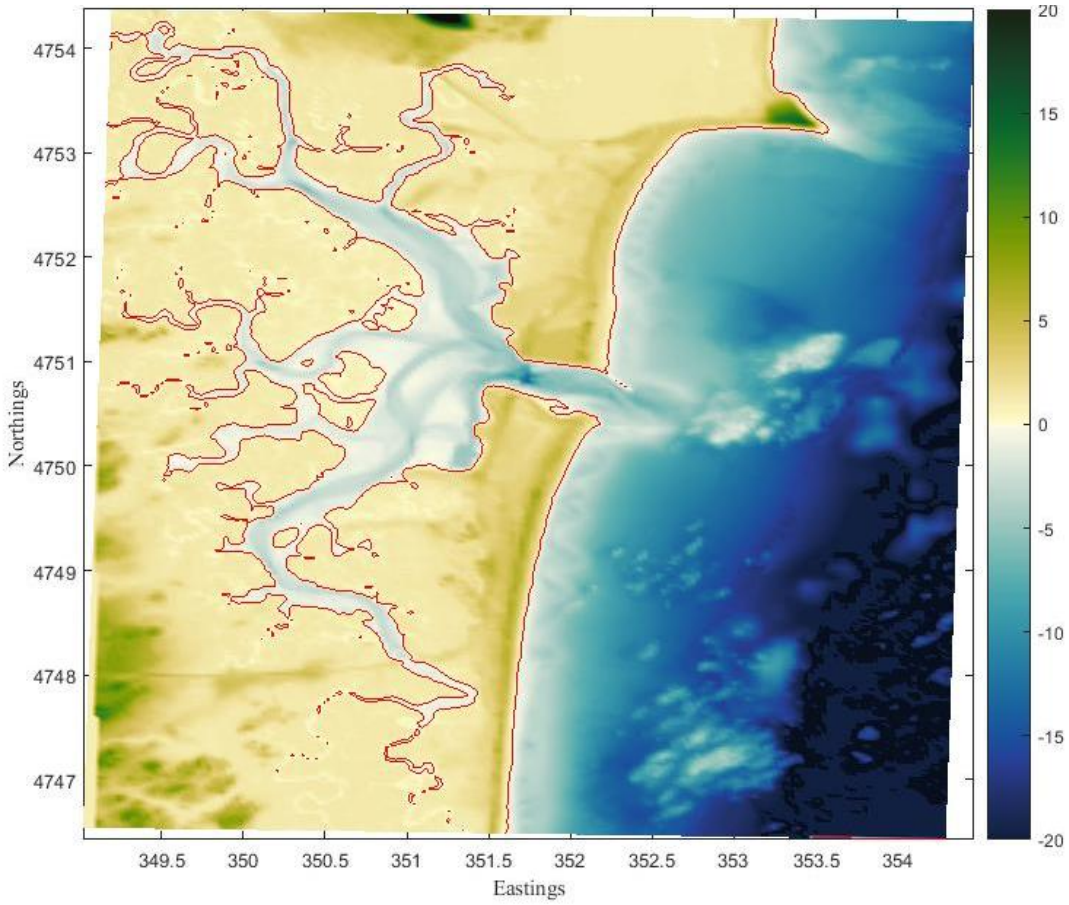

Figure 3.5: Bathymetry of the study area from composite of seven different surveys (described in Appendix A). Elevations are relative to the NAVD88 vertical datum (approximately mean sea level). The red line indicates the 0 m contour. Color scale for depths range between +/- 20 m.

Bed roughness parameters z_o are also established with bottom conditions in the bathymetry grid. z_o is an independent, spatially varying parameter used in the sediment transport equation (3) that determines the velocity profile within the bottom boundary layer important to both dissipation of the flow and initiation of sediment transport. A spatially varying bottom roughness is established in different domains of higher and lower bed roughness by assigning a subset of grid cells within the domain to a prescribed value. These points are then spatially interpolated onto the entire input bathymetry grid. Marsh regions are given a higher bed roughness to account for effects of

subaquatic vegetation, whereas the inlet, flood tidal delta, and tidal channels and creeks are given values roughly dependent on their grain size.

d_{50} (mm)	w_s (mm/s)	ρ_{sed} kg/m^3	Ea kg/m^2/s	τ_{crit} N/m^2
0.03	4.9	2650	5e-5	0.39
0.15	12	2650	5e-5	0.081
0.75	90	2650	5e-5	0.03
3.0	210	2650	5e-5	0.043
0.25	30	2650	5e-5	3

Table 1: Sediment grain size and associated properties defined in sediment transport module in model setup. Grain sizes are determined from grain size distribution curve from sediment grab samples. The fifth grain size (d_{50} = 0.25 mm) represents the hardened structures within the study area and is given a high critical shear stress to inhibit erosion.

The heterogeneous sediment distribution at Hampton is represented by five different sediment size classes, each defined by a grain size diameter d_{50}, critical shear stress for erosion τ_{crit}, fall (settling) velocity w_s, and sediment density ρ_{sed}, and erosion rate parameter, Ea, (Table 1). Settling velocity of each grain size is calculated as a function of the immersed weight of the grain, drag coefficient, C_D, and particle Reynolds number, *Re*, each given by

$$W_s = \sqrt{\frac{4(\rho_{sed}-\rho_w)gd_{50}}{3\rho_w C_d}} \quad (12)$$

$$C_D = 1.4 + \frac{36}{Re} \quad (13)$$

$$Re = W_s \frac{d_{50}}{\nu} \quad (14)$$

where ρ_w is density of water, and ν is the kinematic viscosity. Critical shear stress, τ_{crit}, for incipient motion is calculated based on the Soulsby and Whitehouse (1997) shields fit curve, using the dimensionless grain size, d^*,

$$\tau_{crit} = \frac{0.24}{d^*} + 0.55(1 - e^{(-0.020*d^*)}) \quad (15)$$

$$d^* = d_{50}\left(\frac{g\left(\rho_{sed}/\rho_w - 1\right)}{\nu^2}\right) \quad (16)$$

The erosion rate parameter is based on similar sediment transport studies conducted in back-barrier estuaries along the United States East Coast (Ganju, *et al.,* 2017*)*. Grain sizes are based on a cumulative grain size distribution curve from the 112 sediment grab samples.

Each grid cell of the bottom boundary grid is initialized with a fractional distribution of grain size for each size class (Figure 3.6). Herein, grain size distribution is based on depth, with shallower and tidal flats consisting of finer silts and clays. The upper reaches of the tidal creeks were altered to be dominantly mud (silts and clays). Classifying the grain size distribution by depth was deemed to be an efficient qualitative method to create a reasonable representation of grain size heterogeneity in the system.

There is no established routine within COAWST to represent hardened shorelines within a model domain. However, in HSE three different shoreline stabilization structures are present, including a jetty bordering the north side of the inlet, half-tide jetty bordering the south side of the inlet, and the subsurface bulkheads in the southern end of the Seabrook side to the harbor (Figure 3.6). These structures have an integral influence on the circulation and local stabilization of the sediments. To account for the effect of these hardened shorelines on hydrodynamics and sediment transport within HSE, the bulk properties of the sediment bed layer are configured to represent permanent properties of a hardened (non-erodible) coastal structure.

To represent the hardened structures, a fifth, non-cohesive, grain size class was introduced in which the grain class is characterized by a high critical shear stress to inhibit erosion ($\tau_{crit} = 3.0\ N\ m^{-2}$). In locations of the hardened structures, the sediment size class represents 100% of the corresponding bed cell. The geographical extent of the Hampton Jetty, Seabrook half-tide jetty,

and harbor bulk heads impinging on the Middle Ground are determined through a GIS shape layer obtained from the New Hampshire Department of Environmental Services (NHDES) and from satellite imagery, and matched to the corresponding grid cell locations.

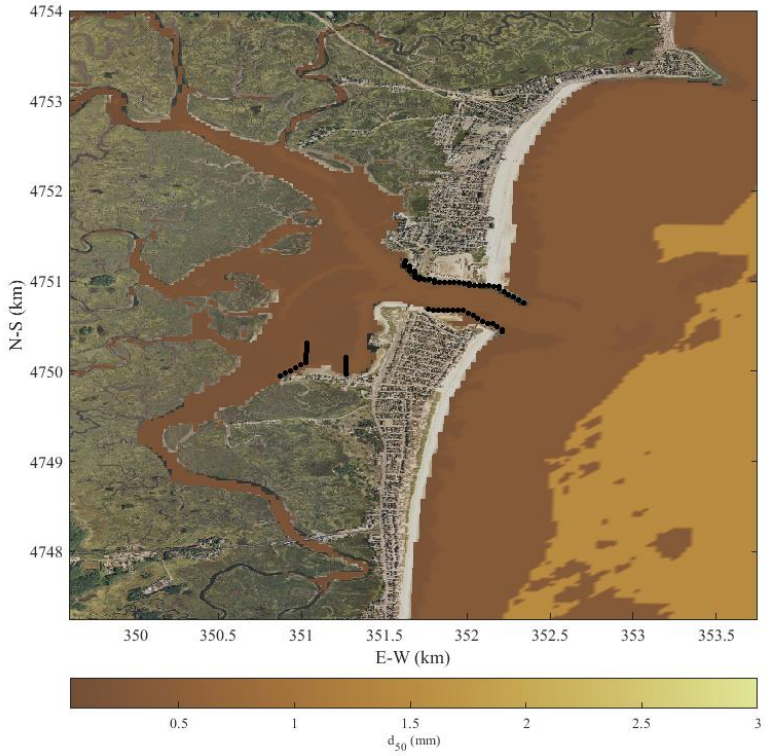

Figure 3.6: Initial d_{50} grain size map based on smoothing of the observed distribution from the grab samples and used for the initial bottom boundary condition in the numerical model. Sub-tidal and hardened structures are represented with solid black pixels.

Apart from where hardened structures are located, the sediment bed is defined to consist of a single layer with thickness of 5 *m* and a porosity of 0.5 (following Warner, *et al.*, 2008a). At the hardened locations, the bed is set to a thickness of 0.001 *m* to discourage sediment from settling and accumulating on the structures.

Forcing Conditions

The hydrodynamic model (ROMS) is forced at the eastern open boundary with sea surface height observations (Figure 3.7) obtained from the NOAA Tide Station 8423898, located roughly 20 *km* north at Fort Point, NH, the entrance to the Piscataqua River (NOAA, 2020). Verified sea surface elevation observations are averaged continuously over six minute intervals, referenced to the NAVD88 vertical datum, and publically available through NOAA's Center for Operational Oceanographic Products and Services (CO-OPS) webpage (https://tidesandcurrents.noaa.gov/).

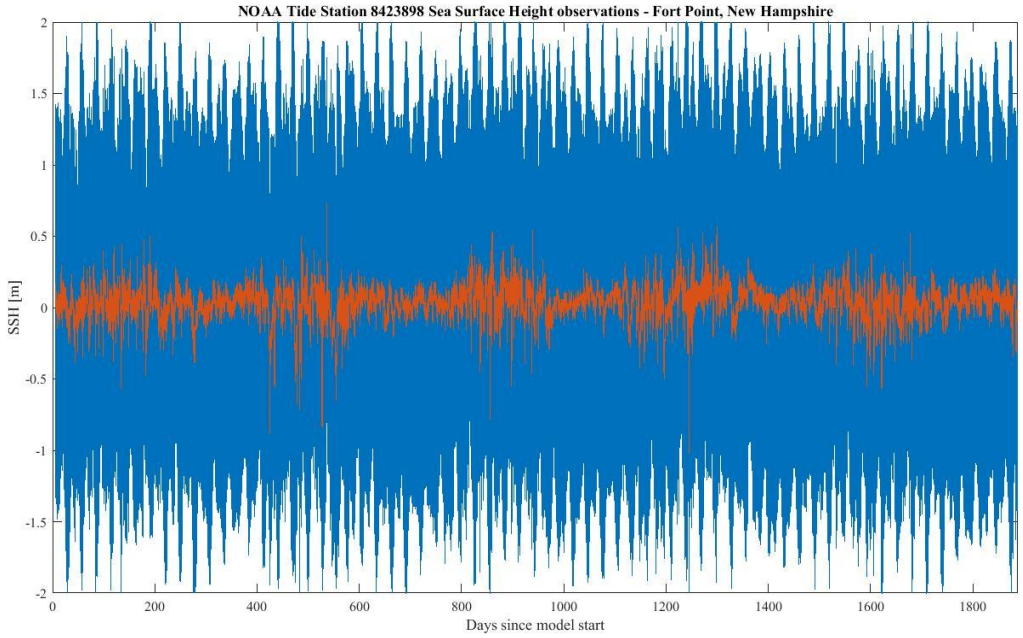

Figure 3.7: Time series of water level elevations relative to MSL used to force the model. Blue represents observed sea surface height and the red indicates subtidal motions due to winds and atmospheric pressures. Subtidal data is calculated by subtracting the dominate tidal constituents from the observed signal.

Water level observations account for the net forcing of tides and weather-driven sub-tidal motions due to winds and atmospheric pressure changes. Comparison of sea surface height observations at Fort Point from 16 Sep to 18 Oct 2011 compare well to those obtained from the pressure sensor on the ADCP deployed just seaward of Hampton Inlet (Figure 3.8) but with a phase

difference of approximately 5-8 *deg* arising from the spatial separation of the two gauges. Water level observations obtained from the Fort Pt. tidal station are converted to netCDF formatted files, and used to drive the model for the 5-year simulations (from 1 September 2011 to 31 December 2016), as well as a 40-day simulation (25 October 2017 to 10 December 2017) used to compare with the field observations of currents and water levels and verify the hydrodynamics in the model. To account for model spin-up time, observational data is ramped up from still water to the full range of water levels using a hyperbolic tangent function spanning 5 days.

3.4 Model simulations

Model simulations are conducted for two cases: (1) 40-day model runs for comparison against 2017 field observation data to verify that the hydrodynamics are adequately simulated, with iteration to determine the sensitivity to viscosity and bottom roughness parameters; and (2) five-year model runs beginning September 2011 to simulate longer sediment transport patterns in HSE and subsequently compare with observed bathymetric change patterns. Using ideal parameters identified through the 40-day model verification runs, five-year sediment transport simulations are initiated to estimate the morphologic change in HSE over longer, multi-year time-scales. Models are ran on a Crap XE6m-200 supercomputer.

CHAPTER 4

RESULTS

4.1 Hydrodynamics

Hydrodynamic data to validate the COAWST model runs were collected between 3 November and 6 December 2017, encompassing an entire spring-neap tidal cycle. Vertical variation of the flow is validated against observations from Station B (Figure 3.2), within the main portion of the harbor. In this comparison, modeled currents are transformed from the sigma coordinate system into the observational Cartesian coordinate system with elevations relative to mean sea level (MSL) and corresponding to bin elevations of the Station B ADCP.

Time series comparison of the north-south and east-west velocity components at 5 elevations relative to MSL are shown in Figure 4.1. The model accurately reproduces variations in the currents throughout the water column, with RMS differences between observation and model simulations at all bin elevations of 20.54 and 17.49 *cm/s* for east-west and north-south velocity, respectively. The RMS errors amount to about a 11-13% error in velocity, similar to other model-data comparisons for the nearby Great Bay Estuary (Cook, *et al.*, 2019). Errors in the model arise from model errors, but also because the bathymetry used in the model simulations was obtained in 2016, whereas the observations were deployed in 2017, about 1 year later. Evolution of the harbor sedimentation patterns between 2016 and 2017 likely resulted in some change in the current speeds and directions at the sensor location between 2016 and 2017. Considering the magnitude of the bathymetric evolution in the harbor over 5 years from 2011-2016 (shown later in Figure 4.2) was about 20-33% of the water depth near sensor B location, we

would expect about a 4-7% change in depth from 2016-2017 (assuming a linear extrapolation in erosion/accretion rate). This change in depth would be expected to have a small effect on the currents, resulting in higher RMS errors.

Cross-spectra between observed and modeled sea surface elevation, and depth-averaged east-west, and north-south currents were computed and are shown in Figure 4.2 with the energy density spectra for the model and data (upper panels), coherency spectra (middle panels), and relative phase spectra (lower panels). Observations and model results show similar energy distribution across the frequency range of the spectra, and reveal the dominant M2 semi-diurnal tidal constituent induced by the resonance in the Gulf of Maine (Garrett, 1972), as well as the diurnal tidal constituents (O1 and K1) and the over-tides (M4, M6, etc.). High coherence is observed at the smoothed tidal frequencies for the sea surface elevation time series, as well as for the orthogonal velocity components. The phase spectra show near zero phase for the dominant tidal components in sea surface elevation records, as well as across frequency space for the velocities. These results suggest that the model is well able to reproduce the dominant flows and water levels within the harbor over the spring-neap tidal cycle, and provide confidence that the modeled water levels and velocities within the harbor for the 5-year simulations are reasonable.

Modeled currents in the narrow tidal channels did not compare well with the observed currents obtained upstream in the Black Water River (I) and Mills Creek (Station E). This result is likely due to coarse spatial grid scales in the model (of 30 *m*) not well resolving the details of the flows in the narrow channels. The modeled bed shear stresses are likely under-predicted as the smoothed bathymetry with coarse grids spreads the volume flux out over larger areas resulting in weaker velocities. The model also cannot resolve the near-vertical banks of the salt marshes, and only approximates the flow fields. As a consequence, the erosion and depositional

Figure 4.1: Time series comparison of modeled currents (red solid line) and observations (black dots) from Station B as a function of elevation relative to MSL. (upper panel) North-south velocity component. (bottom panel) East-west velocity component. Modeled currents were

transformed from sigma coordinates to the elevation of the ADCP bins. RMS values range 20.54 and 17.49 cm/s.

patterns in the salt marshes and upstream tidal channels are not expected to well simulate the sediment transport in those areas. However, the changes to the salt marsh channels and upstream sedimentation patterns are not large, and the limitations of the model upstream would be expected to have minor impact on the sediment transport patterns in the harbor where the velocities are well modeled. Significantly higher resolution models would be needed to model the transport in the salt marshes and tidal creeks, resulting in significant (orders of magnitude) more computational resources, and are considered beyond the scope of the present study.

Time-series comparisons of sea surface elevation between model simulations and observations for the 30 day runs (shown in Figure 4.3) are also used to verify model results at stations A, B, D, E, F, G, and H (locations shown in Figure 3.2). RMS errors between model and observed water level range between 13.61 *cm* and 11.18 *cm*, indicating that the model accurately resolves variations in sea-level height throughout the entire estuary. These RMS errors amount to about a 3% error in estimating water levels, also consistent with results from Cook, *et al.* (2019) for the Great Bay. Miss-matches between the modeled and observed water level fluctuations arising from the 1-year time offset between bathymetric data collection and model simulations are not expected to be large as the details of the water levels are not strongly affected locally by the bathymetric irregularities (an assumption borne out by the small percent errors in water level time series at all locations). It should be noted that data are shown in Figure 4.3 from Station I (located up in the tidal channel of Black Water River), but are not considered in the RMS calculations because the pressure record was offset and did not record water levels at lower stands of the tide.

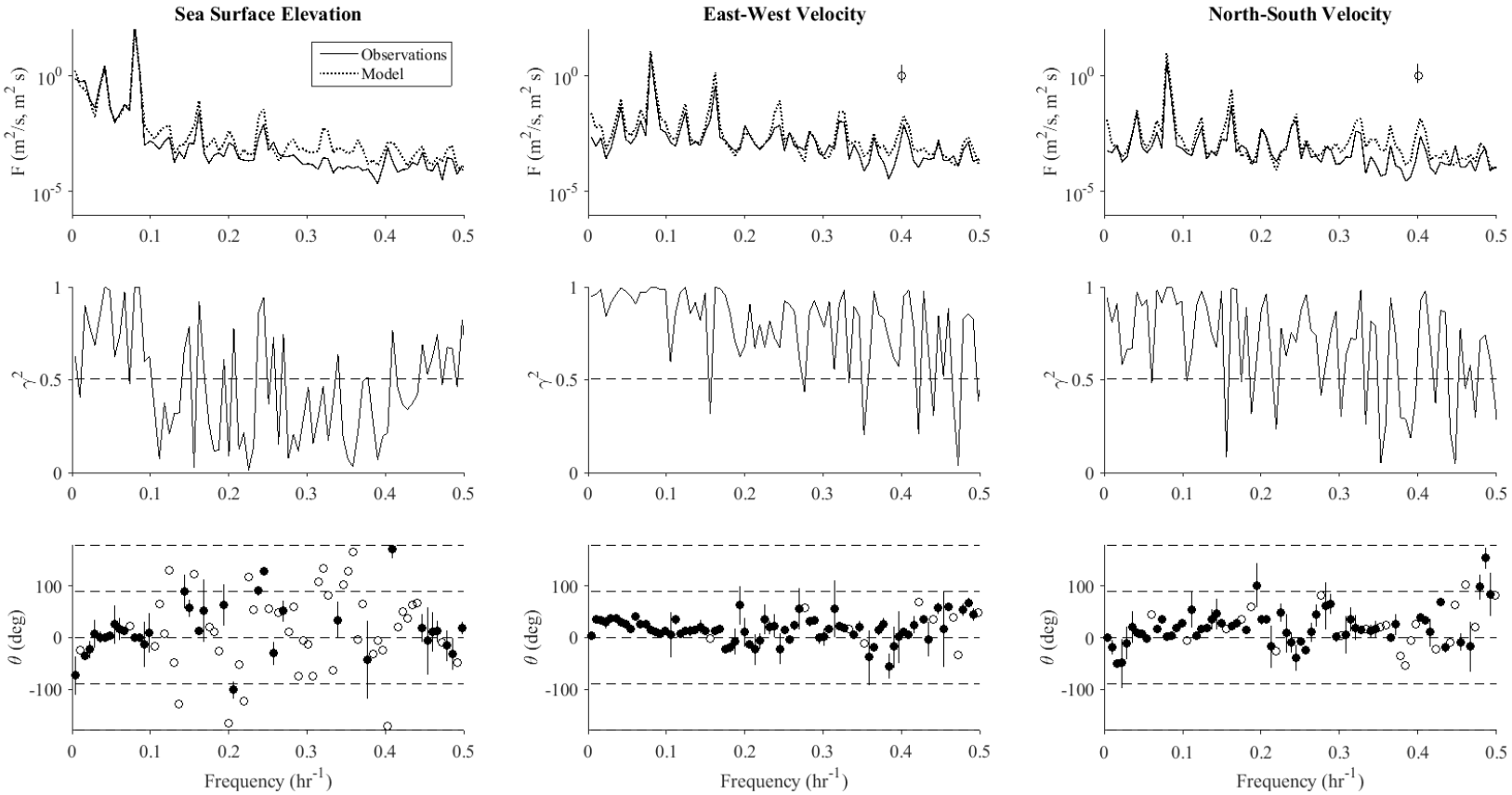

Figure 4.2: Cross-spectra for observed and modeled results from Station B located in the back-bay of the study area. (left panel) shows sea surface election. (center panel) depth-averaged east-west velocity. (right panel) depth-averaged north-south velocity. Confidence interval is shown in the upper center and right panel.

Comparison of energy dissipation of the M2 tidal wave from the inlet to the upper reaches of Hampton River tributary is considered. Using harmonic analysis with T_TIDE (Pawlowicz, *et al*., 2002), amplitude decay and phase lags between modeled and observed water level measurements are compared (Figure 4.4). Following methods described in Cook, *et al.* (2019), the dominant M2 tidal constituent energy is represented by the linear gravity wave relation,

$$E = \frac{1}{2}\rho g A^2 \tag{17}$$

where E is the total energy per unit surface area, A is the amplitude of the M2 tidal constituent, g is gravity, and density of seawater, ρ, is constant. Modeled (lines) and observed (symbols) energy decay and phase change of the principal M2 tidal constituent are shown in Figure 4.4 for the tidal wave propagating along transects following the channel from the estuary mouth to the upper reaches of Hampton River (purple), Mill Creek (yellow), and Black Water River (orange). The energy and phase are normalized by the value observed just offshore the estuary mouth at Station A (Figure 5). The energy decay (tidal dissipation) and corresponding phase changes are small for all channels, and indicate that the tidal wave is nearly completely reflected and acts as a dominantly standing wave. The difference between total energy decay at the upper reaches of the

tidal creek between modeled and observed results is small (about 3 %), indicating that the model simulations accurately capture the tidal behavior throughout HSE.

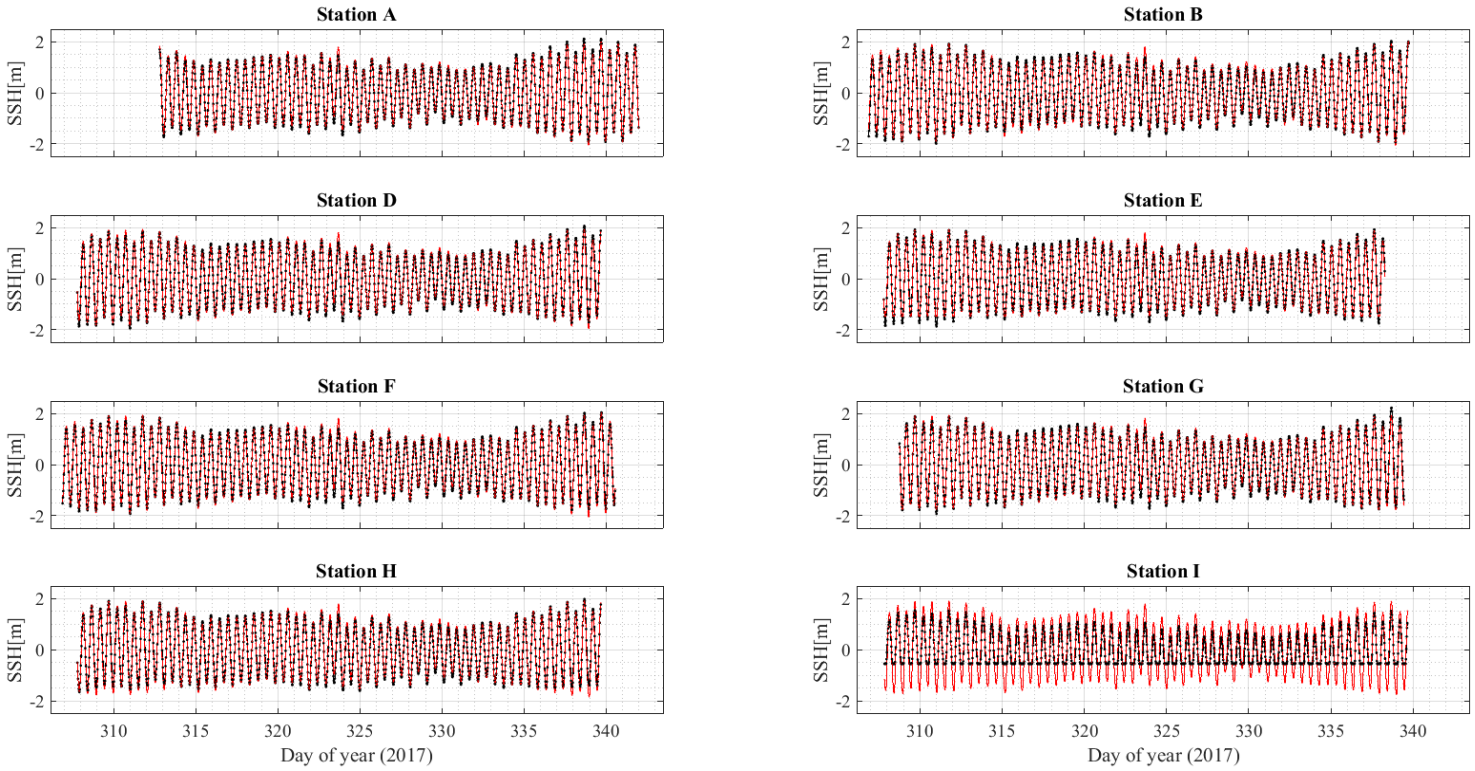

Figure 4.3: Comparison of sea surface elevation time series from model simulations (red) and observations (black) for Stations A, B, D, E, F, G, H, and I. RMS values range 13.61 cm and 11.18 cm Observations from Station I did not include values for lower stands of the tide and are not included in the RMS calculations.

Bottom roughness values in the model are iterated during model simulations and evaluated by comparing best fits of model tidal analysis to observed energy dissipation of the M2 tidal wave. Model results indicate that model simulations best reflect observed conditions with a spatially variable bottom roughness, z_o, rather than a single value. Values of z_o ranged from 10^{-6} near the estuary mouth (Stations A and B) to 10^{-3} upstream near Stations I, E, and G, and were spatially smoothed onto the model grid. This result is not surprising given the heterogeneous nature of the seafloor with generally coarser sands near the inlet transitioning to finer silts and

clays in the upper reaches of the tidal channels where the flows diminish. Iterating over different eddy diffusivity constants showed no significant difference in M2 tidal dissipation, and a single value of 0.00 was used for all calculations.

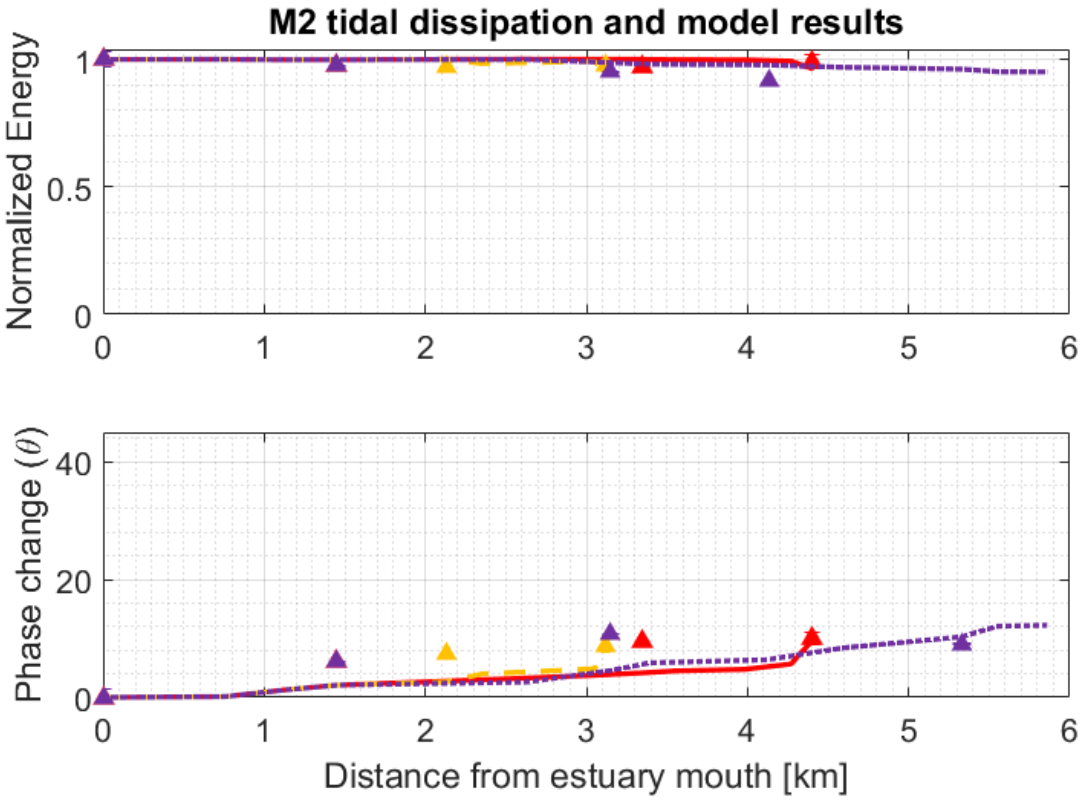

Figure 4.4. Spatial variation of the normalized M2 tidal energy and phase change relative to the offshore location of Station A. Model values are solid and dashed lines with colors indicating different channels (red – southern Black Water River channel; yellow – central Mill Creek channel; purple – northern Hampton River channel). Observations are indicated with the triangle symbols with colors corresponding to the different channels.

4.2 Geomorphic Change

Measured bathymetry surveyed in 2016 is compared directly to the 2011 bathymetry (Figure 4.5) by subtracting the 2016 survey from the 2011 initial bathymetry at model grid points. Significant observed changes to the bathymetry include regions within the flood tidal shoal where new channels are cut along and across the Middle Ground, infilling of the

navigational channel leading to the southern Seabrook Harbor, channel development of the Hampton Harbor and northern channel leading to the Hampton River, and rearrangement of sediments within the Inlet. Net change in water depths range +/- 2 *m* and are shown by the color bar in Figure 4.5. Changes to the bathymetry seaward of the inlet mouth are not known as the 2016 survey did not extend seaward into the Gulf of Maine. Changes to the bathymetry in the narrow channels further up the estuary are generally much less than in the harbors and Middle Ground, but do indicate some (subtle) evolution in the erosional and depositional patterns.

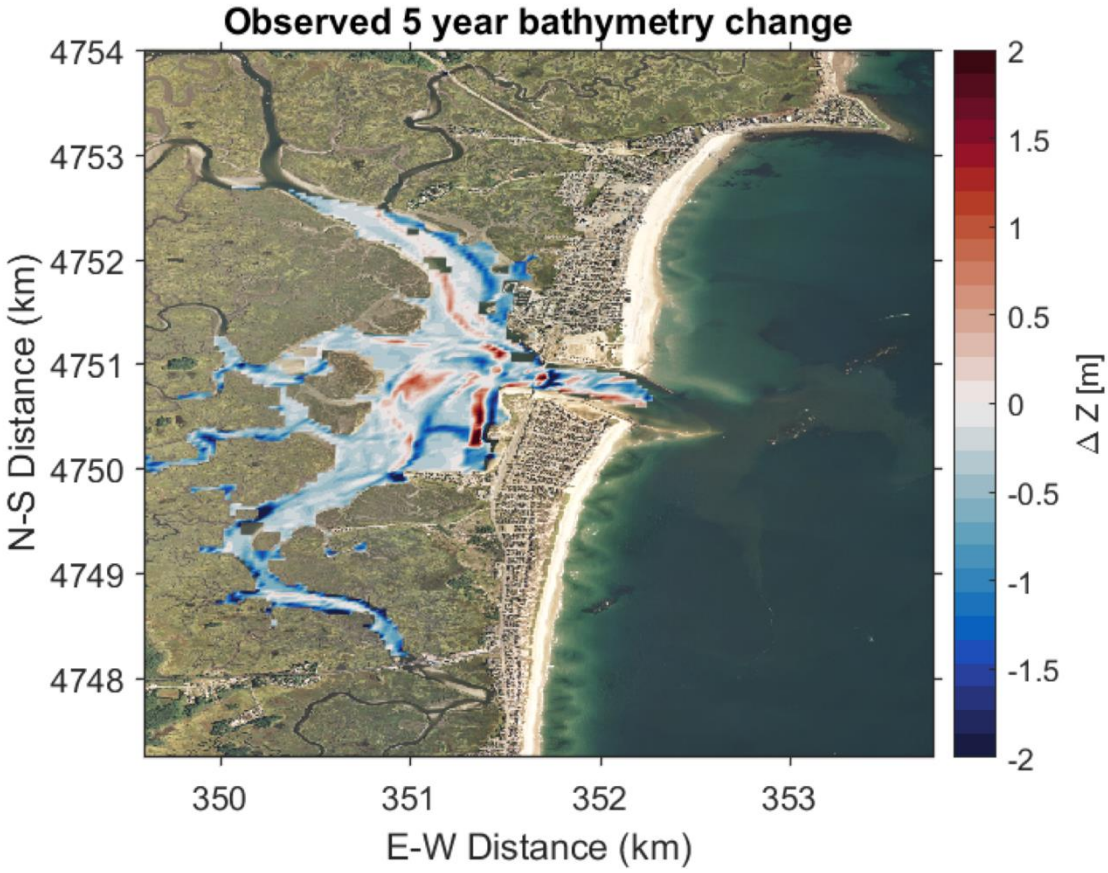

Figure 4.5: Observed changes to seafloor bathymetry between 2011 and 2016. ΔZ determined by subtracting the 2016 survey from the 2011 initial bathymetry grid with elevation change indicated by the color bar (in m). Regions of deposition are shown in red, and erosion in blue.

The end result of the five-year model simulation of sediment transport in HSE is subtracted from the initial bathymetry to show the changes produced by the model (Figure 4.6). The scale of the change in elevation of the seabed in Figure 4.6 is the same as that for Figure 4.5 (showing the observed changes). The model also shows changes to the flood tidal delta with new channels cut along and across the Middle Ground very similar in character as that observed, and shows the strong infilling of the navigational channel leading to Seabrook Harbor. The magnitude of the change in depths is quite similar to the observed values. Model results for the northern channel heading to the Hampton River show development of the channel similar in character to the observations. In particular, there is a deepening of the channel to the south and to the north, with an elongated shoal developing between the two channels. The observed strong deepening of the channel to the north-east (nearer to the Hampton moorage area) is not reproduced by the model. Although the areas of erosion and deposition are not precisely aligned, the general sedimentation behavior is well modeled, and considered a reasonable result considering integration of incremental changes occurring at very small time steps (~1 *s*) over the long, multi-year simulation period.

Although the model also shows rearrangement of the Hampton Harbor flood tidal delta and main channels with depth changes and morphological evolution similar to the observed behavior, upstream in the narrow tidal creeks and in the inlet itself the erosional and depositional patterns that deviate more substantially from the observations. This is not surprising considering that the model grid does not resolve the flow velocities or bed stress in the narrow channels or steep banks of the salt marsh areas.

Within the inlet itself, the depth changes predicted by the model show significant accretion on the north side of the inlet not shown in the data, and patterns of sedimentation of the

main channel not precisely aligned with the observed changes. There are well-known sand waves that migrate into and out of the inlet on both inter-annual and spring-neap tidal cycles with heights of 1-2 *m* and wavelengths of 20-40 *m*, as well as fields of dynamic mega-ripples (0.1-0.3 *m* amplitudes and 1-10 *m* wavelengths) that populate the inlet bathymetry (McKenna, 2013). These bedforms are not well modeled with the relatively coarse 30 *m* grid, and the transport is only approximated with the CSTM model parameterizations. As well, the bathymetric surveys smoothed to the 30 *m* grid also do not well capture those changes.

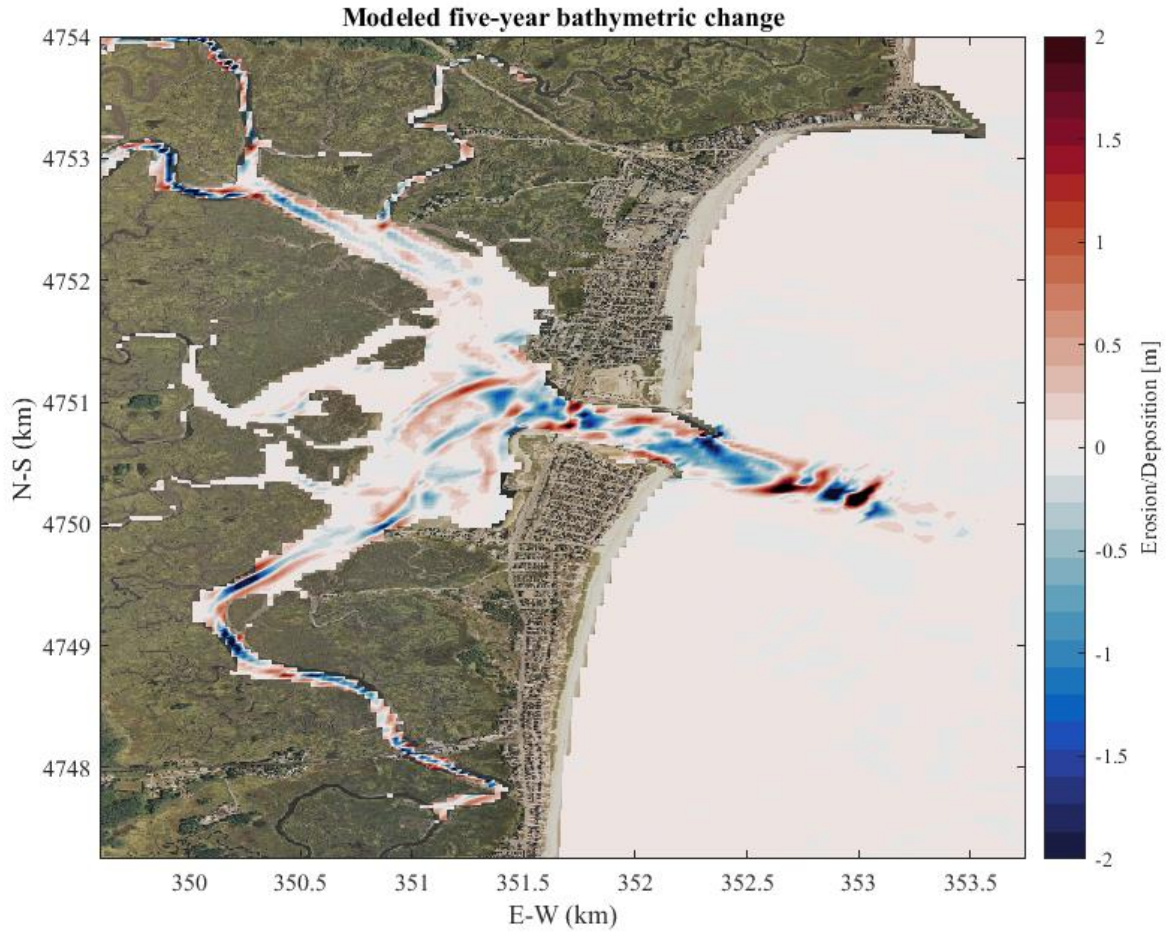

Figure 4.6: Modeled changes to the bathymetry over a five-year period. Same format and color scale as for the observations shown in Figure 4.5

Outside the inlet mouth extending 1.5 *km* offshore, the model shows significant evolution of the ebb tidal delta with apparent large undulations of the seabed with scales of 100-500 *m* and depth changes exceeding +/- 2 *m*. As there were no bathymetric surveys of the ebb tidal shoal in 2016, it is not known if this evolution is occurring. Although ebb-tidal shoals are well known to evolve over time with strong rearrangement by the strong tidal flows in many other areas with similar tidal currents (*e.g.*, at Oregon Inlet, NC; McNinch and Humberston, 2019), the sedimentation patterns and evolution outside the inlet would be expected to be effected by ocean waves and wind-driven shelf currents. In our study, neither of these processes were considered and would need to be addressed with additional modeling and verification from bathymetric surveys. In essence, we are assuming that the sediment transport over the ebb-tidal shoals does not affect the evolution of the flood tidal delta at Hampton.

In general, the model qualitatively reproduced the observed geomorphic changes within the back-bay flood tidal delta, and in particular the cut across the Middle Ground and infilling and narrowing of the navigation channel leading to Seabrook Harbor that led to emergency dredging operations. The model also showed qualitatively that the northern Hampton Harbor, upstream channels, and inlet bathymetry evolved, but with details that do not precisely match the observations.

CHAPTER 5

DISCUSSION

Erosional flux (equation 7) is a source or sink term representing total settling of sediment out of the water column or the upward flux of sediment with the sediment transport module that depends on the model bed shear stress (determined by the hydrodynamics). Two parameters then determine the magnitude of the flux: the average critical bed stress, τ_{ce}, given by equation (13) and the bed erodibility parameter, E_o. The critical bed shear stress is determined by the grain size in the model as well as bulk properties of the seabed (including packing and porosity) that are poorly understood. Iterating on τ_{ce} affects the magnitude of erosion and deposition as the fluid bed stress changes. As critical shear stress of each grain size decreases, the magnitudes of erosion and deposition increase, as shown in Figure 5.1. In these cases, the magnitude of the depth changes increase with decreasing τ_{ce}, as expected, but the spatial pattern does not change appreciably. Similarly, the magnitude of the sediment flux increases and decreases linearly with erodibility constant, with larger changes occurring for larger values of E_o. Rather than iterating on both parameters together, the erodibility parameter was held constant (E_o = 5e-5 kg/m^2/s), and τ_{ce} was varied to see the effects of increasing or decreasing sediment flux.

In the HSE estuary, the sensitivity to τ_{ce} does not alter the spatial pattern of erosion and deposition (*i.e.,* the morphological evolution), but rather the rate at which the channels and shoals form, and will accelerate or delay the transport processes effecting the temporal evolution of the erosion or sedimentation across the delta. This behavior is similar to the effect of morphological scale factors that accelerate the fluxes of sediments to decrease simulation time (see Roelvink and

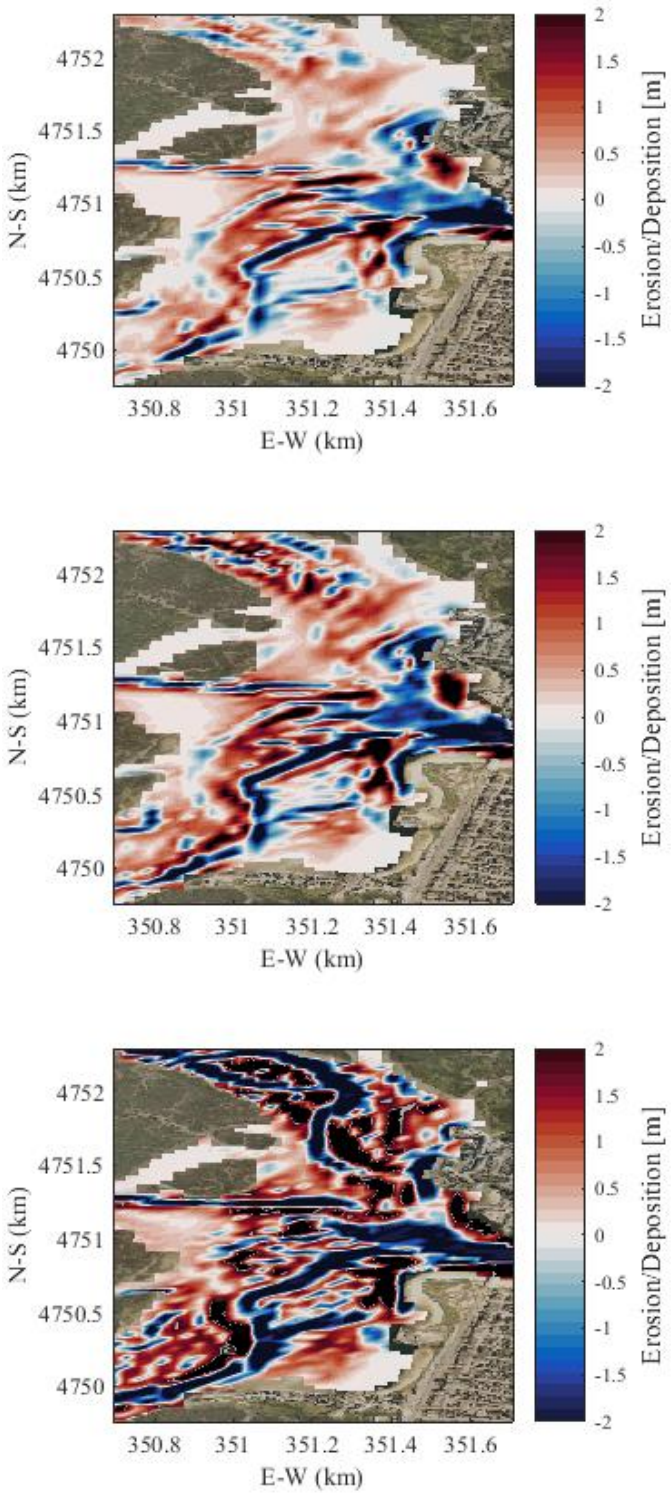

Figure 5.1: Changes to the model results as a function of critical shear stress (top panel) critical shear stress reduced by 25%. (top panel) critical shear stress reduced by 50%. (bottom panel) critical shear stress reduced by 75%. Color scale the same as for Figures 4.5 and 4.6.

Reniers, 2012). At HSE, the value of τ_{ce} effects the timing of when the infilling of the navigational channel will occur. This is expected, as a higher critical shear stress of a sediment grain size also requires a larger bottom shear stress to initiate motion into the water column. Without *aprior* knowledge of the appropriate critical bed stress, the value must be determined empirically limiting the predictive capabilities of the model. Nonetheless, while iterating on different bottom roughness parameters changes the magnitude of erosion and deposition, the spatial patterns of the morphological evolution of the seabed is not strongly affected.

In the model simulations, the spatially varying bed roughness parameter, z_o, was established by iteration through comparison of modeled currents and tidal energy dissipation with observations for a 40-day period. The resulting spatial grid of z_o thus produces consistent flow fields within the harbor (the area of highest interest) and tidal energy decay (weak in HSE) that determines the phasing of the tidal flows (and eliminates unrealistic amplification of the tide in the upper reaches of the estuary).

Model simulations qualitatively reproduce erosion and deposition patterns across the flood-tidal delta of HSE and adequately resolves the gross behavior of the system using a rectilinear 30 *m* grid. However, the model is unable to reproduce observed hydrodynamics and geomorphic evolution of the seafloor in the upper reaches of the tidal creeks where the spatial resolution of the grid does not resolve the flow fields in the much narrower channels (that gradually close out). While reducing the horizontal grid resolution may improve model results in the shallower, narrower tidal creeks, these changes to the model simulation also significantly increase model computation time as both the barotropic and baroclinic time-steps are correspondingly reduced. For example, reducing the model grid from 30 to 10 *m* requires at least an order of magnitude more computational resources (or simulation time), and still will not resolve the narrow channels.

Models with unstructured grids would be beneficial, as well as simulations considering only depth-integrated flows (neither of which is presently allowed within COAWST when the sediment transport is considered).

In the present study, only non-cohesive sediment transport formulations were considered even though size classes for muddy sediments (silts and clays) were included. The finer sediments behave differently than non-cohesive sediments, and require model components that account for flocculation and cohesive bed parameters that presumably would better resolve the sediment transport processes and the subsequent evolution of the seafloor, particularly in the upper tidal creeks of the study area sediments become progressively muddier. While COAWST sediment transport modules can consider calculations for cohesive sediment classes, they were not included in this study as the primary area of interest was in the back-bay where only small mud fractions are observed (5-10% relative to the 90-95% sand size fractions). In any case, the high flows and bed stress within the harbor and inlet winnow away the fine sediments, and reproduce the general evolution of the flood tidal delta.

In HSE, engineering structures are present that were introduced to alleviate sediment transport problems, and include the north jetty at the inlet mouth, the half-tide jetty to the south of the inlet, and the sub-tidal bulkheads on the southern side of Seabrook Harbor (Figure 3.6). The presence of these structures was included in the model by specifying a size class with very small depth range to eliminate accumulation of sediments on the structures, and a very high critical bed shear stress to eliminate sediment from being eroded (mimicking the behavior of the hardened structures). Without the presence of the sub-tidal bulkheads, the sediment transport in the back bay could not be simulated correctly as the cuts across the flood tidal delta appear to be somewhat controlled by their position and depth. Although the bulkheads protect the erosion along the

southern banks of the Harbor, they likely impact the evolution of the flood tidal delta and the infilling of the navigational channel to the Seabrook moorage.

Application of the model to systems such as HSE can be used to alert coastal managers and engineers to future potential dangers to navigation by mariners that may be forthcoming over inter-annual time periods. Models can also assist in determining re-survey and dredging needs at HSE and in other locations, of direct interest to NOAA's Office of Coast Survey who produce navigational charts for navigable waterways and the United States Army Corp of Engineers who oversee dredging activities in U.S. coastal waters. Incorporating numerical model solutions with observations from bathymetric surveys also elucidate sediment transport processes and sediment pathways at site-specific areas, providing a means to assess the effectiveness of coastal engineering practices to alleviate problem areas that affect boating safety and the economics of coastal communities. In addition, numerical models allow for climate change scenarios and storm-induced response to be evaluated for future planning (Lippmann, *et al*., 2020).

CHAPTER 6

CONCLUSIONS

This study presents model simulations of gross sediment transport patterns over a five-year period for the Hampton-Seabrook Estuary using the coupled numerical modeling system COAWST. The model is forced with sea surface elevation observations from a nearby NOAA tide station and includes both tidal and subtidal forces. The bottom boundary is established with observed depth measurements and the sediment transport module is informed by grain size distribution from field studies. In this study, sub-tidal bulkheads and jetties are represented as a non-cohesive grain size with a high critical stress that inhibits erosion.

Field observations of the vertically varying flow field and sea surface elevation over a spring-neap tidal cycle are used to verify model skill. The initial bathymetric grid constructed in 2011 is compared with surveys conducted in 2016 to determine observed bathymetric change over a 5-year period and used to directly compare modeled seafloor evolution to 5-year model predictions. Modelled results of geomorphic evolution of the seafloor are qualitatively consistent with observed bathymetric change of the study timeframe and capture the gross behavior of the back-bay regime (the area of highest interest). Specifically, modeled bathymetric change captured observed rearrangement of the flood tidal delta including infilling of the navigational channel leading to Seabrook Harbor and new channels cut along and across the Middle Ground.

Model performance is improved by iterating on the explicitly defined bed roughness parameter. The resulting grid of spatially varying of z_o captures the observed flow-field through the back-bay and tidal energy dissipation of the estuary. Sensitivity analysis of model results to

critical shear stress of grain sizes influenced the timing and magnitude or erosion and infilling within the study area, the spatial patterns of morphological evolution did not change. The model does not accurately reproduce observed hydrodynamics and observed sedimentation patterns in the upper reaches of the tidal creeks. Here, the spatial resolution the grid is not fine enough to resolve the narrower channels. Additional studies incorporating unstructured grids may improve model performance in the complex upper reaches of the salt marsh.

Geomorphic modelling studies generally focus on short-term evolution of the seafloor during storm induced events or multi-decadal studies leveraging a MF factor to represent longer time scales. This study shows that detailed modeling without MF factors over inter-annual timescales (relevant to monitoring harbor bathymetric evolution by coastal managers and engineers) qualitatively reproduces the spatial patterns of erosion and deposition in the back-bay of Hampton Seabrook Harbor, including the channel development across the flood tidal delta and the infilling of the heavily used navigational channel. Applications of such model systems have the potential to inform coastal management decisions and to better understand complex sediment transport mechanisms.

LIST OF REFERENCES

Booij, N., Ris, R.C., Holthuijsen, L.H., 1999. A third-generation wave model for coastal regions, Part I, Model description and validation. *Journal of Geophysical Research*, 104 (C4), 7649-7666.

Chapman, D.C. (1985). Numerical treatment of cross-shelf open boundaries in a barotropic coastal ocean model. *Journal of Physical Oceanography*, 15:1060-1075.

Chen, C., Liu, H., Beardsley, R.C. (2003). An unstructured grid finite-volume three-dimensional primitive equations ocean model: Application to coastal ocean and estuaries. *J. Atmos. Ocean. Tech*. 20: 159–186.

Cook, S.E., Lippmann T.C., Irish J.D. (2019). Modeling nonlinear tidal evolution in an energetic estuary. *Ocean Modeling*, 136:13-27.

Eberhardt, A.L. Burdick, D.M. (2008). Hampton-Seabrook Estuary Restoration Compendium. *PREP Reports & Publications*, 76. https://scholars.unh.edu/prep/76.

Flather, R.A. (1976). A tidal model of the northwest European continental shelf. *Recent Developments in Numerical Methods for Atmopsheric Modelling*, ECMWF publication: 364-385.

Ganju, N.K., Schoellhamer, D.H. (2010). Decadal-timescale estuarine geomorphic change under future scenarios of climate and sediment supply. *Estuaries and Coasts*, 33:15-19.

Ganju, N.K., Sherwood, C.R. (2010). Effect of roughness formulation on the performanc of a coupled wave, hydrodynamic, and sediment transport model. *Ocean Modelling*, 33 (3-4), 299-313.

Ganju, N.K., Suttles S.E., Beudin, A., Nowacki, D.J., Miselis, J.L., Andrews, B.D. (2017). Quantification of storm-induced bathymetric change in a back-barrier estuary. *Estuaries and Coasts*, 40:22-36.

Garrett, C. (1972). Tidal resonance in the Bay of Fundy and Gulf of Maine. *Nature*, 238, 441-443.

Haidvogel, D.B., Arange, H.G., Hedstrom, K., Beckmann, A., Malonotte-Rizzoli, P.M., Shchepetkin, A.F. (2000). Model evlaution experiments in the North Atlantic Basin: simulations in nonlinear terrain-following coordinates. *Dynamics of Atmopsheres and Oceans*, 32: 239-281.

Hall-Arber, M., Dyer, C., Poggie, J., McNally, J., Gagne, R. (2001). New England's Fishing Communities. MIT Sea Grant College Program, MITSG 01-15, pp. 426.

Harris, C.K., Wiberg, P.L. (2001). A two-dimensional, time-dependent model of suspended sediment transport and bed reworking for continental shelves. *Computers & Geosciences*, 27, 675-690

Hopkins, J., Elgar S., Raubenheimer, B. (2018). Storm impact on morphological evolution of a sandy inlet. *Journal of Geophysical Research – Oceans,* 123(8):5751-5762.

Kedzierski, J., 1993. New Hampshire Dredged Material Management Study, US Army Corps of Engineers, New England Division, Planning Directorate - Sec. 22-Planning Assistance to States.

Lesser, G.R.; Roelvink, J.A.; van Kester, J.A.T.M.; Stelling, G.S. (2004). Development and validation of a three-dimensional morphological model. *Coast. Eng*., 51, 883–915

Letter, J.V., Boyt, W.L., Hetzel S.B. (2005). TABS-MD Hydrodynamic and Sediment Investigation of Hampton/Seabrook Harbor, New Hampshire (A 227 Program Study Report). ERDC/CHL TR-05-XX. Vicksburg, MS: U.S. Army Research and Development Center.

Leung, K.D. (2007) Hydrodynamic modeling of Hampton/Seabrook Harbor, New Hampshire. *Master's Thesis and Capstones*, 271, Https://scholars.unh.edu/thesis/271.

Lippmann, T.C., Smith, G.M. (2009). Shallow Surveying in Hazardous Water. *5TH International Conference High Resolution Surveys in Shallow Water.* Durhan, NH, USA, p. Portsmouth, NH, 2008. Oct 21 – 24.

Lippmann, T.C., Simpson, A.E., Cook, S.E., Kirshen, P. (2020). Effects of sea level rise on modeled storm surge and current speeds in New Hampshire estuaries, *J. Waterw. Port Coast. Ocean Eng.,* 147(2).

Luettich, R.A.Jr., Westerink, J.J., Scheffner, N.W. 1992. ADCIRC: An Advanced three-dimensional circulation model for shelves, coasts, and estuaries, Report 1, Theory and method of ADCIRC-2DDI and ADCIRC-3DL. *USACE Tech. Report DRP-92-6.* https://apps.dtic.mil/dtic/tr/fulltext/u2/a261608.pdf

Luijendijk, A.P., de Schipper, M.A., Ranasinghe, R. (2019), Morphodynamic acceleration techniques for multi-timescale predictions of complex sandy interventions. *J. Mar. Sci. Eng*., 7, 78.

Luan, H.L., Ding, P.X., Wang, Z.B., Ge, J.Z. (2017). Processed-based morphodynamic modeling of the Yangtze Estuary at a decadal timescale: Controls on estuarine evolution and future trends. *Geomorphology,* 290: 347-364.

Mahmutoglu, S. 2001. Hydrodynamic Modeling of the Tidal Flow in Hampton/Seabrook Harbor, NH. MS Thesis, University of New Hampshire, Durham, New Hampshire.

Marchesiello, P., McWilliams, A., Shchepetkin, F (2001). Open boundary conditions for long-term integration of regional ocean models. *Ocean Modelling,* 3:1-20.

McKenna, L. (2013). Patterns of Bedform Migration and Mean Tidal Currents in Hampton Harbor Inlet, New Hampshire, USA [unpublished Masters thesis]. University of New Hampshire.

McNinch, J., Humberston, J. (2019). Radar inlet observing system (RIOS) at Oregon Inlet, NC: sediment transport pathways at a wave-dominated tidal inlet. *Shore and Beach*, 87(1), 24-36.

Meyer-Peter, E., Mueller, R. (1948). Formulas for bedload transport. *Report on the Second Meeting of the International Associate Hydraulic Structure Research*, Stockhold, Sweden: 29:64.

Moriarty, J.M, Harris, C.K., Hadfield, M.G. (2014). A hydrodynamic and sediment transport model for the Waipoa Shelf, New Zealand: sensitivity to fluxes to spatially-varying erodibility and model nesting. *Journal of Marine Science and Engineering*, 2:336-369.

NH Department of Health and Human Services [NHDES] (1994). Hampton Harbor Management Plan. New Hampshire Department of Health and Human Services, Division of Public Health Services, Concord, NH.

NOAA, 2020. "Fort Point, NH Tidal Station 8423898." NOAA tides and currents. Accessed October, 2015. https://tidesandcurrents.noaa.gov/inventory.html?id=8423898.

Pawlowicz, R., B. Beardsley, and S. Lentz. 2002. "Classical tidal harmonic analysis including error estimates in MATLAB using T_TIDE." Comput. Geosci. 28: 929–937.

Pease Development Authority [PDA], 2012. Division of Ports and Harbors Annual Dredge Report. 555 Market Street, Portsmouth, New Hampshire 03801.

Piscataqua Region Estuaries Partnership [PREP] (2019). Piscataqua Region Estuaries Partnership 2018 Annual Report. PREP Reports &Publications, 414, https://scholars.unh.edu/prep/414.

Randall, P.E. (1989). Hampton: A Century of Town and Beach. 1888-1988. P.E. Randall, Portsmouth, NH

Roelvink, J.A., Reniers, A.J.H.M. (2012). A Guide to Modelling Coastal Morphology, World Sci., Singapore.

Skamarock, W.C., Klemp, J.B., Dudhia, J., Gill, D.O., Barker, D.M., Wang, W., Powers, J.G. (2005). A description of the advanced research WRF version 2. NCAR/TN-468+STR, Natl. Cent. for Atmos. Res., Boulder, Colo.

Shchepetkin, A.F., McWilliams, J.C. (2005). The regional oceanic modeling systems (ROMS): a split-explicit, free-surface, topography-following-coordinate oceanic model. *Ocean Modelling*, 9:347-404.

Soulsby, R.L. Damgaard, J.S. (2005). Bedload sediment transport in coastal waters. *Coastal Engineering*, 52: 673:689.

Soulsby, R.L., Whitehouse, R.J.S. (1997). Threshold of sediment motion in coastal environments. *Pacific Coasts and Ports '97: Proc. 13th Australasia Coastal and Ocean Eng. Conf. and 6th Australasian Port and Harbour Conf.*, 1, 145-150.

Tarpley, D., Harris, C.K., Friedrichs, C.T., Sherwood, C. R. (2019). Tidal variation in cohesive sediment distribution in an idealized, partially-mixed estuary. *J. Mar. Sci. Eng.*, 7(10, 334.

Ward, L.G. (2007). Depositional systems on the New Hampshire continental shelf: formation and controlling processes. Geological Society of America.

Ward, L.G.; Irish, J.D.; Knuuti, K. (2013) Physical processes and morphologic changes in Hampton-Seabrook Harbor, New Hampshire: Natural and anthropogenic alterations. *Northeast Section, Geological Society of America Annual Meeting*, 713, https://scholars.unh.edu/ccom/713

Ward, L.G., Irish, J.D. (2014) Morphologic changes of a heavily developed and modified back-barrier system: Hampton-Seabrook Harbor, New Hampshire. *Geological Society of America Annual Meeting*. Vancouver, British Columbia, Canada.

Ward, L.G., McAvoy, Z.S., Johnson, P., Greenaway, S.F. (2015) Use of high resolution bathymetry and backscatter for mapping depositional environments on the New Hampshire continental shelf. *Geological Society of America (GSA) Annual Meeting, Northeastern Section*. Bretton Woods, NH.

Warner, J.C., Sherwood, C., Arango, H., Signel, R., (2005). Performance of four turbulence closure models implemented using a generic length scale method. Ocean Modeling. 8, 81-113.

Warner, J.C., Sherwood, C.R., Signell, R.P., Harris, C.K., Arango, H.G. (2008a). Development of a three dimensional, regional, coupled wave, current, and sediment- transport model. *Computers and Geosciences.* 34, 1284-1306.

Warner, J.C., Perlin, N., Skyllingstad, E.D. (2008b). Using the model coupling Toolkit to couple earth system models. *Environ. Model. Softw*. 23, 1240–1249.

Warner, J. C., Armstrong, B., He, R., Zambon, J.B. (2010). Development of a coupled ocean-atmosphere-wave-sediment transport (COAWST) modeling system. *Ocean Modelling,* 35(3):230-244.

Warner, J.C., Defne, A., Haas, K., Arange, H.G. (2013). A wetting and drying scheme for ROMS. *Computers and Geosciences,* 58:54-61.

Wu, H., Zhu, J. (2010). Advection scheme with 3rd high-order spatial interpolation at the middle temporal level and its application to saltwater intrusion in the Changjiang Estuary. *Ocean Modelling,* 33:33-51.

APPENDIX A

INITIAL BATHYMETRY GRID

The initial bathymetry grid used as input into the numerical model simulations is compiled from a variety of sources. Gridded datasets available online were obtained from the National Ocean and Atmosphere Administration Coast Data Viewer and the University of New Hampshire Center of Coastal and Ocean Mapping (CCOM) Western Gulf of Maine (WGOM) bathymetry compilation. Each survey has a respective acquisition method, resolution, reference geometry, and year collected. Multibeam bathymetry is exclusively from the CCOM WGOM bathymetry dataset and consists of four distinct surveys merged into one. Data acquired from the NOAA Coast Viewer are individual topographic-bathymetric LiDAR data, encompassing both sub-tidal depths and above sea level subaerial areas.

2010 USACE NCMP Topobathy Lidar: Northeast Atlantic Coast

This data is collected as part of the USACE National Coastal Mapping Program under the USACE Joint Airborne Lidar Bathymetry Technical Center of Expertise (JALBTCX). Data collected using a HawkEye II sensor, meets vertical error at 1 sigma standard deviation, has a vertical accuracy of 20 cm, and a horizontal accuracy of 75 cm. Originally acquired to the NAD83 ellipsoid, observations are transformed from the ellipsoid to orthometric heights referenced to NAVD88 using the National Geodetics Survey's GEOID09 model.

2011 USACE NCMP Topobathy Lidar: MA and NH

This data is also collected as part of the USACE National Coastal Mapping Program under the USACE JALBTCX. The data is collected using a Compact Hydrographic Airborne RapidTotal Survey (CHARTS) system, with a 20 cm vertical accuracy and 75 cm horizontal

accuracy. Again, vertical positions are referenced to the NAD83 ellipsoid, and is transformed to NAVD88 with the GEOID03 model.

2013 USACE NAE Topobathy Lidar: Newbury (MA)

Data is collected using a Coastal Zone Mapping and Imaging Lidar (CZMIL) system under the JALBTCX program. Measurements have a reported vertical accuracy of 7.65 cm and horizontal accuracy of 100 cm. Vertical positions are referenced to the NAD83 NA11 ellipsoid and are used to transform to NAVD88 using the GEOID12A model.

2014 - H12696: NOS Hydrographic Survey

Multibeam data is collected with a Reson multibeam sonars on the NOAA ship Ferdinand R. Hassler, managed by NOAA Office of Coast Survey, Hydrographic Surveys Division. Soundings are originally acquired in MLLW, with NOAA Fort Point tide station as datum gear. The high density of lobster gear on the sea floor shows up as artifacts in the data.

2004 Cape Ann Salisbury Beach MA

This data is collected with the R/V Ocean Explorer by Science Applications International Corporation (SAIC), under contract to the University of New Hampshire, with a Reson 8101 MBES (SAIC, *2004)*. Data supported requirements of the USGS.

2015 Rye Ledge to Great Boars Head Summer Hydro 2015

UNH CCOM summer hydro class collected bathymetry from Rye Ledge to Great Boars Head in June/July 2015. Data is acquired with a Kongsberg EM2040 MBES aboard the R/V Coastal Surveyor and is originally gridded to 1 m horizontal resolution.

U.S. Coastal Relief Model - Northeast Atlantic

A small portion of the model domain seaward of the Hampton Inlet contained no recently collected data. Bathymetry measurements here are acquired from the United States Coastal

Relief Model for the Northeast Atlantic, itself an integrated bathymetry set acquired from a variety of sources and gridded to a 90 m horizontal resolution (DOC/NOAA/NESDIS/NCEI 1999). Due to the large horizontal cell size, no effort was made to establish a common vertical datum in processing as the uncertainty in the elevation value exceeds differences between vertical datums. This data acquired was absorbed within the comprehensive CCOM Golf of Maine bathymetry, subject to quality assurance. The subset of this bathymetry data did not cover an area of primary concern in the thesis modeling studies and thus was accepted as accurate, despite vertical uncertainties.

Creating the Bathymetry Grid

A single, comprehensive bathymetry grid is created in three steps: (i) geometric transformation of bathymetry datasets, (ii) merging of datasets, and (iii) quantitative visual inspection of data quality.

NAD83 UTM Zone 19N and the North American Vertical Datum 1988 (NAVD88) form the geometric basis for the comprehensive bathymetric grid. Data from the NOAA Coast Viewer is downloaded as such while the multibeam data is in WGS84 Web Mercator horizontal datum and Mean Lower Lower Water (MLLW). Using ESRI ArcGIS Spatial Analysis toolbox, the multibeam data is reprojected to the NAD83 UTM Zone 19N and bathymetry depths were adjusted by +1.38 m (check number, it is from the NOAA tidal station) into NAVD88.

Individual datasets are merged using Global Mapper into a comprehensive bathymetry grid with an 8 m resolution. Where there is overlap between data sets, priority is given to the 2011 LIDaR data as it has the largest footprint and allows for 5-year comparison to the 2016 single-beam data. Following preference is given to 2013 LIDar, 2010 LIDaR, and finally the CCOM

multibeam data. Using Global Mapper tools, remaining gaps in the comprehensive grid are interpolated to create a smooth dataset.

In the merging and interpolation process in creating a single comprehensive grid, precision and accuracy of the bathymetric dataset is inherently lost. In effort to best represent the most likely elevation measurement, adjustments were made when necessary. Here, the height of the north Hampton Inlet jetty is raised from below to above sea level. The resulting elevation is based of the most recent LIDaR data. Furthermore, adjustments to the resulting bathymetric grid are made to ensure a smooth numerical solution. Here, tight flow restrictions adjacent to bridges were deepened and widened.

Finally, the comprehensive dataset is saved as a geotiff. Bathymetry is inputted into COAWST numerical model as 30 *m* NetCDF file. Using MATLAB routines, the data is converted into a xyz file, with Eastings, Northings, and depth in positive meters. The combined bathymetry grid is processed with the MATLAB Easygrid routine (https://www.myroms.org/wiki/easygrid) to create a 30m rectilinear gri